DOKUZ EYLÜL UNIVERSITY

GRADUATE SCHOOL OF NATURAL AND APPLIED SCIENCES

DESIGN AND PERFORMANCE EVALUATION OF A COMPOUND PARABOLIC COLLECTOR

by

Paşa YAMAN

January, 2020

İZMİR

DESIGN AND PERFORMANCE EVALUATION OF A COMPOUND PARABOLIC COLLECTOR

A Thesis Submitted to the
Graduate School of Natural and Applied Sciences of Dokuz Eylül University
In Partial Fulfillment of the Requirements for the Degree of Master of Science
in Mechanical Engineering, Thermodynamics Program

by

Paşa YAMAN

January, 2020

İZMİR

M.Sc THESIS EXAMINATION RESULT FORM

We have read the thesis entitled **"DESIGN AND PERFORMANCE EVALUATION OF A COMPOUND PARABOLIC COLLECTOR"** completed by **PAŞA YAMAN** under supervision of **PROF. DR. SERHAN KÜÇÜKA** and we certify that in our opinion it is fully adequate, in scope and in quality, as a thesis for the degree of Master of Science.

Prof. Dr. Serhan KÜÇÜKA

Supervisor

Assoc. Prof. Dr. Alpaslan Turgut

(Jury Member)

Asst. Prof. Dr. Özay AKDEMİR

(Jury Member)

Prof.Dr. Kadriye ERTEKİN

Director

Graduate School of Natural and Applied Sciences

ACKNOWLEDGEMENTS

Foremost, I would like to express my sincere gratitude to my advisor, Prof. Dr. Serhan KÜÇÜKA, for the continuous support of my M.Sc. study and research and for his patience, motivation, enthusiasm and immense knowledge. His guidance helped me in all the time of research and writing of this thesis. I could not have imagined having a better advisor and mentor to my thesis.

My special gratitude goes to Sistem Enerji Üretim San. Tic. Ltd. Şti. which supported financially my M.Sc. thesis and I gratefully thankful for Mert ÇİMEN who manufactured the experimental set up and helped me for technical issues throughout the experiments.

I thank my fellow lab mates in Laboratory of Fluid Mechanics, Azat SERVER, Uğur BÜYÜKTUNCER and Mustafa UYĞUN. And, I am especially thankful for thermodynamics laboratory technician, Alim ZORLUOL, who solved the technical issues during the assembling the experimental system.

This thesis was supported within the scope of Dokuz Eylül University Scientific Research Project, "Bütünleşik Parabolik Güneşli Toplayıcıların Performans Değerlendirmesi" (Grant Number: 2017.KB.FEN.020).

Finally, I wish to express my gratitude to my parents, Seval and Hasan YAMAN. I am so grateful for their support and encouragement.

Paşa YAMAN

DESIGN AND PERFORMANCE EVALUATION OF A COMPOUND PARABOLIC COLLECTOR

ABSTRACT

Compound parabolic concentrators (CPC's) are widely popular solar collector type among concentrated solar power applications. These collectors basically are comprised of reflector and absorber surfaces. Differently from parabolic trough collectors, it does not involve a sun-tracking mechanism. It is possible with CPC solar panels to obtain hot fluid in terms of domestic and industrial use.

In this study, a CPC which has an evacuated tube heat pipe as absorber, was designed and optically analyzed. The reflector of the CPC was truncated from evacuated tubes horizontal axis. A model, which is made of an absorber and a reflector, was optically analyzed by ray analysis so that an optical efficiency for rays at different incidence angles, was calculated. Then, a prototype CPC solar panel in which designed CPC was used, was installed. Utilization of evacuated tube heat pipe decreased the amount of working fluid in the solar panel and the step in time was also shortened. In the experiments, the solar irradiation on the collector, inlet and outlet temperature of water was measured. The solar energy to collector's surface and energy transferred to water was compared and collector's efficiency was calculated at experimental conditions.

In conclusion, using the instant values of optical efficiency and solar irradiation, the solar energy on surface of the absorber tube of CPC was calculated during the day. Calculations were repeated monthly and annual thermal energy production capacities were obtained. The results show that energy absorption capacity of evacuated tube with reflector is more than twice that of evacuated tube without reflector.

Keywords: Compound parabolic concentrator, solar energy, optical efficiency, ray tracing, evacuated tube heat pipe

BÜTÜNLEŞİK PARABOLİK TOPLAYICI TASARIMI VE PERFORMANS DEĞERLENDİRİLMESİ

ÖZ

Bütünleşik parabolik toplayıcılar (BPT) yoğunlaştırılmış güneş enerjisi uygulamalarında oldukça yaygın kullanılan bir güneş toplayıcı tipidir. Bu toplayıcılar temel olarak yansıtıcı ve yutucu yüzeylerden oluşmaktadır. Parabolik oluk tip toplayıcılardan farklı olarak, güneş takip mekanizması içermeyen basit yapılı sistemlerdir. BPT'li güneş panellerinin kullanılması ile evsel ve sanayi amaçlı sıcak akışkan elde edilmesi mümkündür.

Bu çalışmada, yutucu olarak vakum cam tüp kullanılan bir BPT'nin tasarımı yapılmıştır. BPT'nin yansıtıcısı, vakum tüpün yatay ekseni hizasından kısaltılmıştır. Yansıtıcı ve yutucudan oluşan modelin sanal ortamda ışın analizi yapılarak farklı geliş açılarındaki optik verimi hesaplanmıştır. Ardından, tasarımı yapılan BPT'lerin kullanıldığı prototip bir güneş enerjisi paneli hazırlanmıştır. Isı borulu vakum tüp kullanılmasıyla panelde kullanılan su miktarı azaltılmış ve devreye girme süresi kısaltılmıştır. Yapılan testlerde panel üzerine düşen ışınım değerleri ve su giriş ve çıkış sıcaklıkları ölçülmüştür. Toplayıcı yüzeyine gelen güneş enerjisi miktarı ile suya aktarılan enerji miktarı oranlanarak deney şartlarındaki panel verimi hesaplanmıştır.

Son olarak, optik verim ve güneş ışınımının anlık değerleri kullanılarak bütünleşik parabolik yansıtıcı kullanılan toplayıcı yüzeyine gelen güneş ışınımı hesaplanmıştır. Hesaplamalar aylık olarak tekrarlanarak yıllık ısıl enerji üretim kapasitesi elde edilmiştir. Sonuçlar BPT'nin yıllık enerji toplama kapasitesinin yansıtıcı yüzey kullanılmayan vakum cam tüpün enerji toplama kapasitesinin iki katından fazla olduğunu göstermektedir.

Anahtar kelimeler: Bütünleşik parabolik toplayıcı, güneş enerjisi, optik verim, ışın izleme, ısı borulu vakum tüp

CONTENTS

Page

LIST OF FIGURES

Page

LIST OF TABLES

Page

CHAPTER ONE
INTRODUCTION

Renewable energy resources have been remarkably popular due to environmental degradation of fossil fuels. In many countries, energy investments are made on behalf of renewable resources such as solar, wind, geothermal, hydropower, biomass and hydrogen. However, solar energy is much more well-known for small scale applications as a result of its lower installation costs. Electricity production, water heating, air heating, food drying, and solar lighting are the main application areas of solar energy.

In concentrated solar power (CSP) systems, mirrors and high reflective surfaces are used to gather sun light into a small area to obtain useful heat. Generated useful heat is converted to electricity in a power generator. Installation and operation costs of these systems require a big amount of capital so that government support is usually needed. Parabolic trough, heliostat, fresnel, and parabolic dish concentrators are well-known CSP systems. Superheated working fluid which is more than 400°C is possible to produce with CSP systems.

As a result of the high cost of CSP systems, compound parabolic concentrators (CPC) are proposed as low-cost and easy-to-apply systems. CPC's are solar thermal concentrators which have not a sun tracking system. Concentrating sunlight without having a sun tracker makes the cost much lower. Compound parabolic concentration system is applicable in numerous areas such as solar water heating, solar air heating, illumination, and water disinfection. CPC's are classified according to their absorber surface shape such as flat, triangle, oval, fin and circular. The current thesis focused on optical and thermal properties of CPC with vacuum tubes. In the following section, an extensive research in terms of compound parabolic concentrator has been made and a wide overview from the current literature on theoretical and experimental applications has been provided.

1.1 An Overview of the CPC in Current Literature

Earliest studies of compound parabolic concentrators had been carried out throughout the instrument experiments for Cherenkov radiation. A development made by (Hinterberger & Winston, 1966). Moreover, an independent and parallel development arisen in Russia (Baranov & Melnikov, 1966) Their potential as concentrators for solar energy collectors was revealed by (Winston, 1974). Figure 1.1 illustrates a CPC with a tubular absorber in which sun rays are reflected.

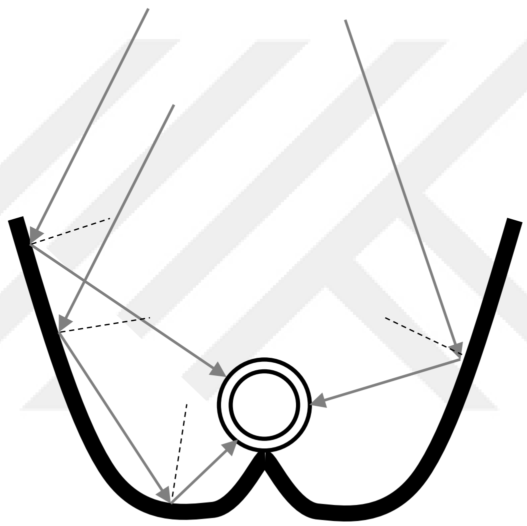

Figure 1.1 Sketch of compound parabolic concentrator with reflected rays at different incidence angles

Compound parabolic concentrator is a non-imaging solar collector. It is appropriate for applications such as water heating, space heating, solar air conditioning, refrigeration, desalination, industrial process heat, steam generation, distillation of essential oil, solar driers, and even solar cooking. It is important to add on that applications of CPC are not limited to the previously mentioned research areas, there may be new applications under ongoing research (Sonawane & Bupesh Raja, 2017). CPC's application temperature is generally ranges 150°C to 200 °C. It is composed of a reflector and an absorber. Hence, reflection and absorption coefficients act much decisive role on optical efficiency of the collector which influence eventually thermal efficiency.

Directing the sun rays to the target area will decrease optical losses so that overall efficiency will be improved. The reasons for efficiency losses are incorrect settlement of the collector, design fault and low coefficients of reflection, transmission and absorption. Due to its geometrical structure, sun tracking is not required in order to perform a concentration. Eliminated expenditure of the sun tracking mechanism allows cost effectively to manufacture and install the CPC. In this chapter, studied CPC systems in the current literature are presented.

Bellos, Korres, Tzivanidis, & Antonopoulos (2016) investigated in their study the thermal and the optical performances of the compound parabolic concentrator with an evacuated tube. The results of the design study showed that an optimum aperture width is 300 mm, focal length 50 mm and diameter of absorber is 34 mm. The authors emphasized that shape of the involute of the concentrator has not a considerable effect to the overall efficiency. Collector's optical efficiency was determined in terms of different solar angles, such as transversal and longitudinal. Fluctuations in transversal angles lead to decreasing in optical efficiency. The decrease in optical efficiency signifies a requirement to use a sun tracking system in order to reduce angular fluctuations and increase optical efficiency. In thermal analysis, two well-known thermal fluids (high pressure water and regular thermal oil) were utilized to examine in contrast. High pressure water displayed better performance and it is the most appropriate fluid for transferring heat, due to higher values of conductivity and lower values of dynamic viscosity give rise to higher heat convection coefficient. The temperature distribution over the absorbing surface and in the thermal fluid was determined, and it was validated by a virtual model designed with a 3D CAD software. Moreover, a flow simulation was accomplished.

Liu, Tao, Lu, & Wang (2014) proposed a steam generator consisted of a simplified compound parabolic concentrator which is easy to be manufactured, cost-friendly and simple to operate. The simplified CPC can generate steam in a temperature up to 200°C and 0.55 MPa pressure. The proposed system of simplified CPC's has a total aperture area of 32 m^2 and consisted of 60 collectors. Each collector has an all-glass vacuum tube, simplified CPC, and metal concentric annular tube. This makes it preferable and low-cost alternative in concentrating sun light. When the irradiance is greater than 650 W/m^2 in sunny days, efficiency is generally more than 30%. However, the system's overall efficiency is about 32% with a temperature of 200°C steam. Superheated steam above 150°C can be generated for 3 hours at noon and saturated steam for 6 hours. System's output power is 8-11 kW for 3 hours at noon.

Wang, Yu, Jiang, Yang, & Liu (2016) proposed a new V-shaped form in CPC. In accordance with the edge ray principle, concentration ratio and gap efficiency were discussed in the proposed model. The CPC was put in a glass tube, and it was called inner CPC. Solar collector's parameters such as optical efficiency, reflectance, transmittance, and absorption ratio were analyzed. Optical efficiency was divided into two; direct and diffuse optical efficiency, in order to obtain a valid result. Incidence angle was divided into transversal and longitudinal incidence angle. Different CPC models with various gap sizes have been developed and analyses were carried out by ray trace program, TracePro. It was found out in simulations that, determinant factor for the gap efficiency was connected more to gap size, than incidence angle. Optical analysis of the designed CPC was carried out based on incidence angle, direct and diffuses irradiance flux. Overall optical efficiency was about 50%. It was claimed that when the diffuse irradiance ratio is increased, the overall optical efficiency will decrease down to 30%. In the analysis absorptance, reflectance and transmittance ratio were taken as 0.91, 0.88 and 0.89, respectively. According to these parameters and size of the gap, the CPC model was analyzed and it was proved that new V-shape form which is used instead of involute bottom has promising future.

Kim, Han, & Seo (2008) tried to investigate and develop the thermal performance of CPC with an evacuated tube. In terms of outlet temperature, net irradiance flux on the absorber and thermal efficiency, regular CPC collector was compared with one axis tracking CPC. From the point of maintenance, using a CPC with internal reflector is much more applicable compared to CPC with an external reflector. With the help of a mechanical tracker, one axis tracking CPC's aperture was always vertical to sun rays, so that sun rays could be absorbed with minimum loss. In the numerical model, the experimental system was simulated using parameters such as the thickness of reflector, outer tube, inner tube and copper tube. Apart from numerical code, TracePro software was used in order to obtain the connection between the incidence angle and irradiance flux. After that, the numerical model has been built and analyzed in terms of irradiance data. 100,000 rays were traced by TracePro for the regular and one axis tracking CPC's, in the interest of direct irradiance intensity and incidence angle. It was proved that the larger the incidence angle, the lower the direct irradiance intensity on the absorber. On the basis of measured and computed data, it was clear that the developed numerical model is able to predict precisely the thermal performance of the collector. The results showed that the thermal efficiency of the one axis tracking CPC collector is 14.9% higher than regular CPC collector. It was added that higher outlet temperatures would be possible if the absorber diameter could be smaller.

Wang, Li, & Liu (2015) studied solar vacuum tubes with truncated CPC in order to provide hot air (150°C~230°C) for industrial production. Air heating system included 30 connected solar collector units. Each unit consisted of a truncated CPC, solar vacuum tube and embedded concentric copper tube heat exchanger. Space between vacuum tube and copper tube was filled with stainless steel mesh layer. CPC was made of stainless steel mirror plate and welded directly to the steel shelf. Air was pumped consistently by a compressor with a constant initial temperature. It was stated that concentrating efficiency of a CPC with flat absorber decreases by about 15% in comparison with CPC with involute. Optical efficiency of the CPC was obtained about 51% based on reflectivity, transmissivity, absorptivity, dust stratification and gap loss. After air entered the system, it was heated increasingly through 30 solar collectors. It was noted that number of collecting units do not affect the peak temperature, only at the mass flow rate of air and the output power. At the 30th unit, air reached 230°C at noon at an irradiance of 920 W/m^2. Air temperature decreased quickly afternoon depending on irradiance degradation. It was observed that air temperature surpassed the 160°C for 3 hours at noon. Experimental analysis proved that tested CPC unit, even in Winter, has perfect collecting performance and output power. Thermal efficiency of the solar collector has decreased based on increase in air temperature. Thermal efficiency is 52% at an air temperature of 70°C, 35% at 150°C and 21% at 220°C.

Gudekar, Jadhav, Panse, Joshi, & Pandit (2013) proposed a model of CPC for the process steam generation. The proposed CPC would be of interest in contrast with a parabolic trough and a flat plate collector with respect to cost effectiveness and lower production cost. Several types of CPC's (traditional, truncated) have been produced to understand the working principle for water heating and steam production. To reduce the disadvantages of traditional CPC, parabolic curves above the focal point were cut out and curves below focal point were selected. The proposed model has an acceptance angle of 6°, tilt arrangement was performed once a day and aimed to generate steam up to 150°C. 30 units were installed in two rows and total aperture area was 60 m^2. Inlet and outlet of piping, tank, and pump were insulated by glass wool. Water was distributed through the main pipe of the system. The temperature and irradiance of the system were recorded steadily. After the steam was generated, it was re-pumped to the tank and water-steam mixture has been separated. Steam was taken from the top of the tank and flow rate was measured. At first, experiments were carried out without a glass envelop on the absorber tube, that is why it took too much time to reach boiling point. For instance, experiments which were carried out in January, (without glass envelop) it took 2.5 hours to reach 100°C and flow rate of steam was 3~3.5 kg/h. The reason for a long time and the low flow rate was heat loss. After modifying the system with borosilicate tubes, in April, it took 1 hour 50 minutes to reach 100°C and flow rate started at 7 kg/h and reached 10 kg/h. Solar irradiance was measured 700 W/m^2. In conclusion, proposed CPC is easy to manufacture, worked rationally for steam production and modifications in the system will reduce heat loss and enhance irradiance gathered at the aperture.

Buttinger, Beikircher, Pröll, & Schölkopf (2010) offered a non-tracking flat plate solar collector with 1.8 concentration ratio. The suggested collector was adjusted in the east-west direction, and comprised of absorber and reflector. Reflector's bottom part was preferred to be V-shaped, owing to its popularity in practice, in order to minimize ray losses. A research was carried out to choose an appropriate acceptance angle and concentration ratio for annual high energy yield. It was shown that a contrast lies between acceptance angle and concentration. In the experiments, the collector was filled in with air, argon or krypton gas, with a pressure of 10 mbar. The lowered pressure inside allows minimizing heat losses, mostly by convection and conduction. Lowering pressure resulted in that heat losses were reduced with air by 50% and with krypton by 75%, in comparison with air at 1 bar. Glass surface and bottom of the collector were supported with multiple parallel metal sheets against each other so that stability of the collector's case could be provided. Sealing must be carried out carefully so that the collector's low pressure environment can endure at least 10 years. In the prototype, two types of seals were used in the outer and inner part. Polysulfide was utilized as outer material owing to its low gas permeability and resistance, and polybutylene rubber inside due to its low gas permeability, weather and UV resistance. A prototype which has an aperture area of 2 m^2 was tested in Munich in summer. Results showed that 50% efficiency with krypton at 0.01 bar and 40% efficiency with air at 0.01 bar was reached for 150°C temperature with a global irradiance of 1000 W/m^2.

Ustaoglu, Okajima, Zhang, & Maruyama (2016) designed a non-tracking thermal collector which was consisted of a compound parabolic and an involute reflector. The concentrator was aligned in the east-west direction and leaned southward. A comparison was made between single and dual concentrator in an evacuated tube. In order to prevent absorber's heat loss, it was enclosed with a vacuum tube. Dual concentrator enhanced the availability of collecting more rays. However, when a ray gets through the glass, its intensity is decreased as much as surface's transmissivity. Using a vacuum tube around dual concentrator increased collected solar irradiance marginally by 28%. Using a dual concentrator in vacuum tube could be suggested for utilization in a collector unit due to reduced constituent cost. Ray tracing was performed for a two dimensional model. 52% of rays arrived in the aperture of the single concentrator and 82% of rays for the dual concentrator. The average optical efficiency of single concentrator was 37% and of dual concentrator was 57%. Thermal efficiency for dual concentrator was greater by 21% at a gray surface absorber temperature of 373 K. Besides, it was proved that the system could be run for high temperature applications such as steam production owing to high surface temperature. Ignoring the end effects, yearly and seasonal performance results showed that dual concentrator had better performance. However, during summer and winter solstices, both of concentrators' performances dropped owing to lowered solar irradiance. That is why a seasonal arrangement of the concentrator is required in order to enhance the collection of irradiance.

Aguilar-Jiménez, Velázquez, Acuña, López-Zavala, & González-Uribe (2018) studied CPC's with a concentric tube which was aligned in different positions (E-W and N-S) with a tilt angle of 32°. Designing, modeling, assembling, experiment, and validation of the CPC's were involved in the study. Acceptance angle 24.3°, concentration ratio 2.22 and length of the CPC was accepted 2 m. Reflector, transparent cover, absorber, and concentric tube were made of aluminum, polycarbonate, copper with selective surface and copper, respectively. A thermal model was developed using an existing mathematical model which was created before. Thermodynamical equations were solved with EES (Engineering Equation Solver). Two pieces of collector units were built from four CPC's in order to implement experiments. A metal stall was constructed in order to support collector units in E-W and N-S directions. A comparison between thermal model's and experiment's results made and an average difference of 1.76°C for N-S CPC and 2.19°C for E-W CPC was demonstrated. With a mass flow rate of 2.4 kg/min, N-S CPC reached its maximum temperature with a difference of 6°C and E-W CPC with 5.5°C, with a mass flow rate of 2.4 kg/min. The reached maximum temperature differences dropped to 1.8°C for both of the collector units with a mass flow rate of 6.2 kg/min. Instantaneous efficiency and heat gain results for E-W CPC and N-S CPC were 34% - 742 W and 36% - 793 W, with an average irradiance of 980 W/m^2. The results showed that CPC in the E-W direction had an optical efficiency of 57.5% and CPC in the N-S direction had 51.3%. Heat loss coefficient is higher in E-W CPC than N-S CPC. Dissimilarities in efficiency, heat loss and reached maximum temperature depend on incidence angle and fluid dynamics.

Singh, Redpath, Aboutorabi, Kattakayam, & Griffiths (2010) investigated utilization of CPC collector units in order to heat water for settlements in northern maritime climate. Owing to more diffuse irradiance in the north, flat plate solar collectors are of no use. That is why, it is important to gather sun rays, both direct and diffuse, for water heating. Two types of CPC were developed, one of them had heat pipe as the absorber, the other had a regular circular pipe as the absorber, with a concentration ratio of 1.82. Heat pipes are believed to be resistant to freezing and reduce heat losses. Developed CPC’s have been supported with an adjustable surface between 40° to 70°. Absorber and aperture areas of the manufactured CPC’s are 0.102 m^2 and 0.186 m^2. The developed models were investigated for 20°C, 30°C, 40°C and 50°C inlet temperatures which are appropriate temperatures for regular solar water heater systems. 800 W/m^2 irradiance affected the heat pipe CPC and after 75 minutes, absorber surface reached 80.3°C and reflector reached 42.9°C, in a steady state. For regular CPC, absorber surface and reflector temperature results were similar. Overall thermal losses of the CPC’s generally have been formed due to natural convection from hot absorber plate to the reflectors and glass cover. Two systems showed similar collector efficiencies as 58% for inlet temperatures of 40°C and 50°C. It was shown that regular CPC had better performance in northern maritime settlements with lower irradiance (<600W/m^2) and lower inlet temperatures (<50°C). It was proven that regular CPC is much more suitable for domestic usage where ~50°C hot water is required. It is significant to include that cheaper manufacture cost of regular CPC’s makes it more preferable.

Widyolar, Jiang, Ferry, & Winston (2018) investigated CPC collector with a non-traditional absorber surface. In the beginning, a circular absorber surface was designed, however owing to production restraints, new geometry for absorber was demanded. A pentagon-shaped absorber was used in glass envelope in order to gather concentrated rays. In terms of gap loss, customized absorber and simplified reflector, 93% geometrical efficiency was reached in comparison with regular CPC. Pentagon shape was made of copper and covered with the commercial selective surface, SunSelect. It had an absorptance of 0.95 and emittance of 0.05 at 100°C. A copper pipe was welded with ultrasonic welding technique on the top and bottom of pentagon-shaped substance as U-tube. Glass envelope was made of borosilicate glass with a transmittance of 0.92. Mylar, commercial reflector film, was selected with reflectance of 0.89 and covered over aluminum sheet. Proposed model is totally vacuumed and sealed under 10^{-4} mbar. Oil was selected as the working fluid. Manufactured model had an aperture area of 4.5

m^2 whereas simulation showed optical and thermal efficiencies were assumed to be 71% and 50% at 200°C, respectively; however, experimental results partly approved that optical and thermal efficiencies are 62% and ~50% at 200°C, respectively. And it reached to a stagnation temperature of 333 °C. A detailed financial analysis presented that collector unit could be built in for $0.58/Watt and heat could be obtained for 3.01 cent per kWh. Entire test area (45.6 m^2) was installed for $13,700 except installation costs which had installed power of 20 kW. The results emphasize that cost for obtaining useful heat is equal to the cost of natural gas in the United States. Utilization of carbon-free energy sources could be possible by increasing popularity and decreasing cost with compound parabolic concentrators.

Jadhav, Gudekar, Patil, Kale, Panse, & Joshi (2013) presented a new prototype of CPC which was truncated without decreasing the concentration ratio. Experiments were carried out to determine peak temperature and collector's thermal efficiency. It was mentioned that one disadvantage of the CPC is its height. Authors have studied to eliminate this disadvantage by modifying geometry of the collector. Traditional CPC has two different focal points which belong to the two different parabolas. However, modified design suggested that two parabolas will have a common focal point which is at the axis of symmetry. Axis of parabolas will be leaned to each other and the angle between two axes will be the acceptance angle. The part below the focal point was used as CPC. Modified CPC was located in E-W direction and tilted southward. A construction was built to support whole concentrating reflectors. Sixteen units were assembled and it has a total aperture area of 94.08 m^2. Circulation system had a storage tank and 400 W pump. Absorber surface had 48 mm diameter and was coated with commercial selective surface (Solkote) which has 85% absorptivity. After that, absorber pipe was enveloped with two glass pipes which have 60 mm and 70 mm diameters, respectively, in order to reduce heat loss by convection. Concentric glass pipes were not evacuated. The results for absorber tube without and with glass tubes are as the following; average thermal efficiency was 25.7% & 34.2% and average steam generation rate was 27 kg/h & 34.5 kg/h, respectively. It was detected that thermal efficiency increased (35% to 42.3%) depending on increment in direct normal irradiance intensity (577 W/m^2 to 707 W/m^2). A few experiment showed that thermal efficiency is independent from fluid flow rate at the same outlet temperature and same solar irradiance.

Santos-González, Sandoval-Reyes, García-Valladares, Ortega, & Gómez (2014) designed a compound parabolic concentrator based on one-dimensional numerical model. In the numerical model continuity, momentum and energy equations were solved for the inside and the wall of the absorber tube. Moreover, an overall thermal analysis was performed in the solar concentrator. Submitted model was truncated owing to the costs of manufacture and material. A system which is consisted of 12 CPC's was built and had an aperture area of 2.1 m^2. Concentration ratio of the system is 1.8 and had an acceptance angle of 30°. Tubular absorber was coated with selective surface and had an absorptance of ~90%. Low-iron tempered glass was used as cover on the collector and had 91% transmittance. Compound parabolic reflector surface had 90% reflectance and coated with anodized aluminum. After that, a ray trace analysis was carried out in order to demonstrate optical losses as a result of truncation. Tonatiuh, an open source software, was used to trace rays. Optical analysis showed that ~42% of the reflector were cut, however only ~7% of the rays were lost due to truncation. System had two water storage tanks, recirculation pump and supporting construction which is able to change collector's tilt angle. Experiments were carried out under an average solar irradiance of 940 W/m^2 and average outdoor temperature of 35.2°C. Water was selected as working fluid and tests were performed in temperature of 30°C~60° and mass flow rate of 2~12 kg per minute. The highest increase in temperature was 7°C at the mass flow rate of 2 kg/min, inlet and ambient temperature of 42.5°C-35.6°C, irradiance of 1054 W/m^2 and the lowest increase was 1°C at the mass flow rate of 10 kg/min inlet and ambient temperature of 42.4°C-36.7°C, irradiance of 927.5 W/m^2. The maximum energy gain of the collector was 1.47 kW at the mass flow rate of 12 kg/min and irradiance of 1026 W/m^2. It was observed that pressure drop increased with higher mass flow rate due to friction. It was found that highest pressure drop was 1.2 kPa at the mass flow rate of 12 kg/min. Experimental results were compatible with the Mexican Standard of NMX-ES-001-NORMEX-2005, so that the system can generate hot fluid at stable temperatures for process heat.

Jiang, Widyolar, & Winston (2015) presented a new characterization method to determine system's performance without using flow rate and thermal measurements. In the experiments, XCPC (external CPC) with pentagon shaped absorber had 4.5 m^2 area and ICPC (integrated CPC) with 3.5 m^2 area were compared. ICPC hosted an 8 mm diameter heat pipe on fins inside a vacuum tube and fins had selective coating while bottom half part of the vacuum tube had reflective coating. In the system, mineral oil was utilized as the working fluid. Mineral oil works in low pressure environment, so that a simpler plumbing system is required. However, it is a flammable fluid, that's why plumbing system's sealing against leaking must be perfect. Moreover, in terms of lower heat transfer capability of the oil compared to water required rapid working velocities. Flow meter and heat capacity measurement tools' results lead to fluctuations on the values due to change in temperature, errors in the system and oxidation by the time. Insulation was applied to calorimeter to minimize heat loss and errors to be below 2%. It was found that heat capacity of mineral oil was 10%~20% more than the values supplier gave, owing to oxidation. By using new measurement system, variations on the values of flow rate and heat capacity of mineral oil were stabilized by using parameters such as voltage, current and temperature. Results showed that XCPC and ICPC had thermal efficiencies of 52% and 42% at 200°C, respectively.

As it was seen, various articles show that studies have been executed as numerically, analytically and experimentally. In this thesis, study of the CPC was made by analytically and experimentally. In the following chapters, solar energy and its applications containing the CPC has been presented and some experimental data was obtained. After that, annual heat generation capacity was comparatively calculated between axially truncated CPC.

The chapters of the thesis are as in the following: In chapter 2, a detailed information was given about solar irradiation and solar angles and calculation of transversal and longitudinal components of incidence angle was shown. A general information about solar collectors was also given. In chapter 3, the design of CPC was made and design steps for Solidworks were explained, calculation of optical efficiency, thermal efficiency and total energy gain was shown. In chapter 4, experimental setup was described, the design method for CPC rib was shared, the operation principle was given and instant solar irradiation, thermal efficiency and the results of the experiments were given. In chapter 5, annual performance comparison was made for evacuated tube with and without reflector. The contribution of reflector to total energy gain was showed.

CHAPTER TWO
SOLAR ANGLES, DEFINITIONS AND APPLICATIONS

In this chapter, solar angles and solar energy applications are explained and general information was provided. Moreover, a classification of solar collectors was made in terms of sun tracking.

2.1 General Properties of Solar Energy

The Sun is a gaseous sphere which is in the middle of the solar system. It has a diameter of ~$1.390x10^8$ m and is far away about ~$1.5x10^{11}$ m from the earth. The Sun has an inclination angle of 7.25°. On account of Sun's imperfect form, different rotation rates occur at different parts, such as 25 days at the equator and 36 days at its axes. It is made of 91% hydrogen and 8.9% helium with regard to the number of atoms. However, in terms of mass, the sun is about 70.6% hydrogen and 27.4% helium. Core energy of sun is transmitted to the convective zone (below the surface) in 170000 years so that its temperature drops to $2x10^6$ °C. It has a surface temperature of ~5500 °C and a core temperature of ~$14x10^6$ °C (Solar System, n.d.).

The solar constant is the received energy at the perpendicular surface of the atmosphere in direction of sun ray's path. The emitted irradiation from the sun's surface has almost a constant value due to spatial relationship between the sun and the earth. Before sending satellites to the space, predictions of solar irradiation's intensity had to be made from the earth's surface. Initial research was accomplished by C. G. Abbot and his colleagues at the Smithsonian Institute. Abbot's estimation of solar constant (G_{sc}) was 1322 W/m^2, however, after studies were carried out, the value was updated to 1367 W/m^2 (Duffie & Beckman, 2013).

Sun emits solar energy with electromagnetic waves which is defined as the solar spectrum. In Figure 2.1, solar spectrum ranges between 290 nm and 2500 nm and it is divided into three variations which are ultraviolet light (290 nm ~ 380 nm), visible light (380 nm ~ 780 nm) and infrared light (780 nm ~ 2500 nm). Overall energy is carried by these light bands according to their capability. %2 of solar energy is carried by ultraviolet light, 47% by visible light and 51% by infrared light. The lower the wavelength, the stronger the energy is. Therefore, ultraviolet light can cause sunburns on human skin. In longer wavelength such as visible light and infrared light, low energy is radiated and it is less harmful (Solar Spectrum, n.d.).

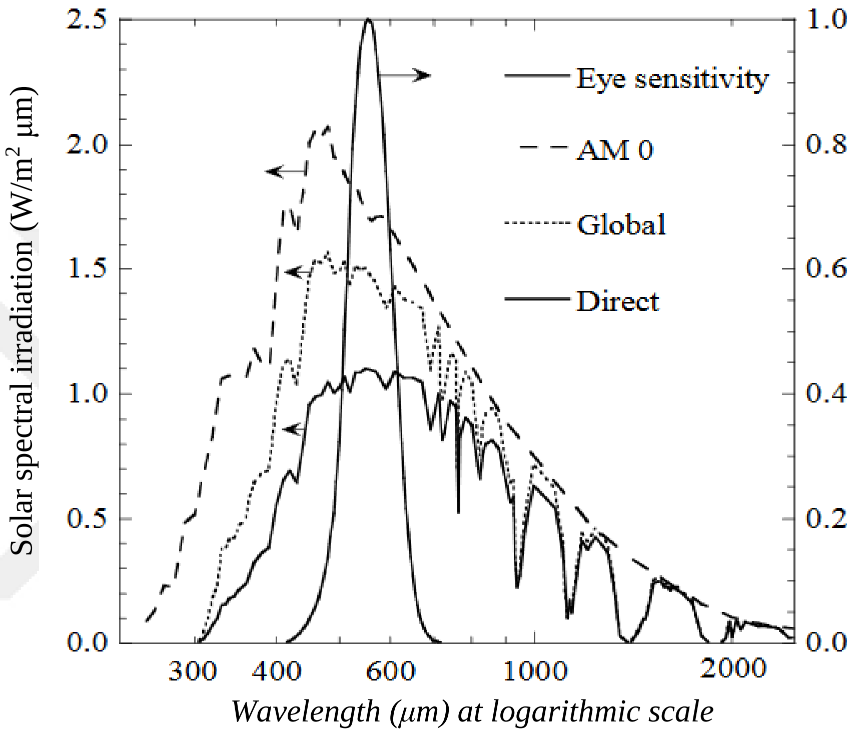

Figure 2.1 Spectrum of the solar irradiance (Brogren, 2004)

The most recognized devices for measuring the intensity of solar irradiation are pyrheliometer and pyranometer. Figure 2.2 illustrates a pyrheliometer, which is used to measure direct solar radiation around its surrounding. In order to attain an accurate result, it is important to face the absorber surface of pyrheliometer directly to the sun. It is widely used in solar tracking mechanism in order to measure direct irradiation. On the other hand, utilization of pyrheliometer is popular to divide global irradiation into direct and diffuse irradiation.

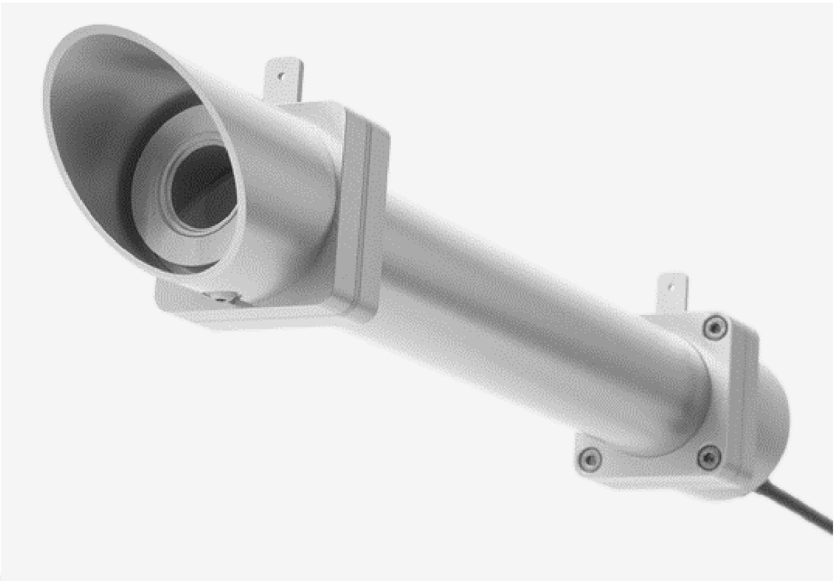

Figure 2.2 Pyrheliometer (Huksefluxusa, 2019)

The working principle of a pyrheliometer is based on temperature difference of the two blackened Manganin cords which are attached to two thermocouples. One of the cords is heated with electrical current, the other one is heated by sun light. When the two cord are at the same temperature, it is known that both cords are heated by the same amount of energy. Solar energy is equal to the energy which was used to heat the first cord. Solar irradiation absorbed by second cord is calculated by dividing the electrical energy with the cord area and its absorptivity (Tiwari & Shyam, 2016).

Figure 2.3 shows that a pyranometer is used to measure global solar radiation on a horizontal surface. Placing pyranometer directly to the sun is of no use, since the primary objective of a pyranometer is to measure the global irradiation on a surface. It is made of a black metal which involves zinc-constantan thermocouples. Thermocouples has the hot and cold parts and hot part is assembled close the black metal and cold part is protected from the sun light. The main principle of the pyranometer is that the hot part is heated due to global irradiation and a temperature difference occurs between hot and cold part. The temperature difference forms a voltage value. Then, this value is converted and read in W/m^2.

Figure 2.3 Pyranometer (Essearth, 2019)

Recently developed silicon type pyranometers are easy to use for all weather conditions. Their fast response time and low cost gives an important opportunity for researchers. The sensor of the pyranometer receives solar irradiation from its surrounding and a small voltage is output, then it is converted into W/m² (Kipp & Zonen Brochure n.d.)

2.1.1 Solar Definitions

G_{on} is the extraterrestrial radiation received on the plane normal to the radiation on the particular day of the year, where n is the number of the day and G_{sc} is the value of solar constant which is 1367 W/m^2 as in Eq. (2.1) (Spencer, 1971).

$$G_{on} = G_{sc}\left(1 + 0.033\cos\frac{360n}{365}\right) \tag{2.1}$$

Direct irradiation arrives to the earth's surface from the sun without having been reflected by the atmosphere. Diffuse irradiation arrives to the earth's surface from the sun after being reflected in the atmosphere. Global irradiation is the total amount of direct and diffuse irradiation on a surface. Solar time depends on angular movement of the sun. Solar noon is the time that sun is over the observer's meridian. In calculations, it is significant to convert standard time to solar time by following equation (Duffie & Beckman, 2013).

$$\text{Solar Time} = \text{Standard Time} + 4\left(L_{st} - L_{loc}\right) + E \quad (2.2)$$

$$E = 229.2(0.000075 + 0.001868\cos B - 0.032077\sin B - 0.014615\cos 2B - 0.04089\sin 2B) \quad (2.3)$$

$$B = (n-1)\ \frac{360}{365} \quad (2.4)$$

where L_{st} is the standard meridian for the local time zone, L_{loc} is the longitude of the location, E is the equation of time in minutes, n is the number of the day in a year; and B is a variable (Duffie & Beckman, 2013). Number of the day can be obtained from Table 2.1, which was created by (Klein, 1977).

Table 2.1 Recommended average days for months and values of n by months (Klein, 1977)

Month	n for *i*th day of month	For average day of month		
		Day of Month	n	Declination Angle
January	i	17	17	-20.9
February	31+i	16	47	-13.0
March	59+i	16	75	-2.4
April	90+i	15	105	9.4
May	120+i	15	135	18.8
June	151+i	11	162	23.1
July	181+i	17	198	21.2
August	212+i	16	228	13.5
September	243+i	15	258	2.2
October	273+i	15	288	-9.6
November	304+i	14	318	-18.9
December	334+i	10	344	-23.0

2.1.2 Solar Angles

Intensity of the sun rays differs relying on season, location, time and Earth's sloped axis. Thus, Sun's angle is directly effects the total gained energy around the Earth. Influence of seasonal variation of the sun rays' intensity is triggered by the Earth's slope and it is resulted in temperature deviation in different seasons (Duffie & Beckman, 2013).

Figure 2.4 illustrates solar angles on a sloped surface. They play an important role in the calculation of the total gained energy. Latitude (ϕ) is the angular location of north or south equator, which varies between -90° and +90°. Declination (δ) is the angular position of the sun at the solar noon with regard to the surface of equator and varies between -23.45° and +23.45°. Slope (β) is the angle between a plane and horizontal surface, varies from 0° to 180°. Surface azimuth angle (γ) is the divergence angle between the local meridian and the normal to the surface, varies from -180° to +180°, 0° means surface faces south. Hour angle (ω) is the displacement of the sun due to earth's movement on its axis, 15° per hour. Negative in the morning, positive in the afternoon. Incidence angle (θ) is the angle between direct ray and normal of the surface. Zenith angle (θ_z) is the angle between normal to the horizontal surface of equator and direct ray from the sun. Solar altitude angle (α_s) is the subsidiary of zenith angle. Solar azimuth angle (γ_s) is between projection of direct ray from the sun on the horizontal surface and the south. Shortly, deviation angle from the south. East of south is negative, but west of south is positive. It is important to keep it in mind that sign of directions in solar angles are as in the following; north and west are positive, east and south are negative (Duffie & Beckman, 2013).

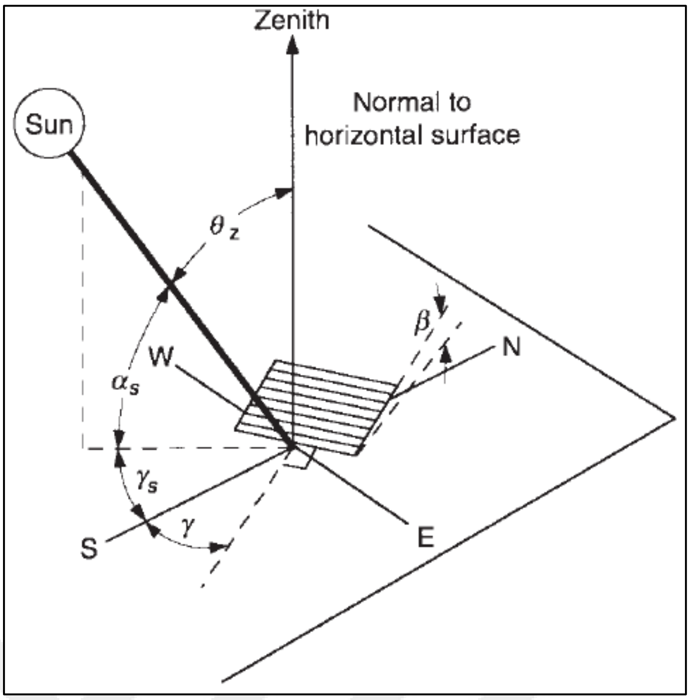

Figure 2.4 Solar angles for a sloped surface (Duffie & Beckman, 2013)

(Cooper, 1969) offered an equation to calculate the declination angle as it is followed in Eq. (2.5) and it is shown in Figure 2.5. It is positive in north hemisphere and it ranges -23.45° to +23.45°. In vernal and autumnal equinox, it is zeroized.

$$\delta = 23.45 \sin\left(360 \frac{284+n}{365}\right) \tag{2.5}$$

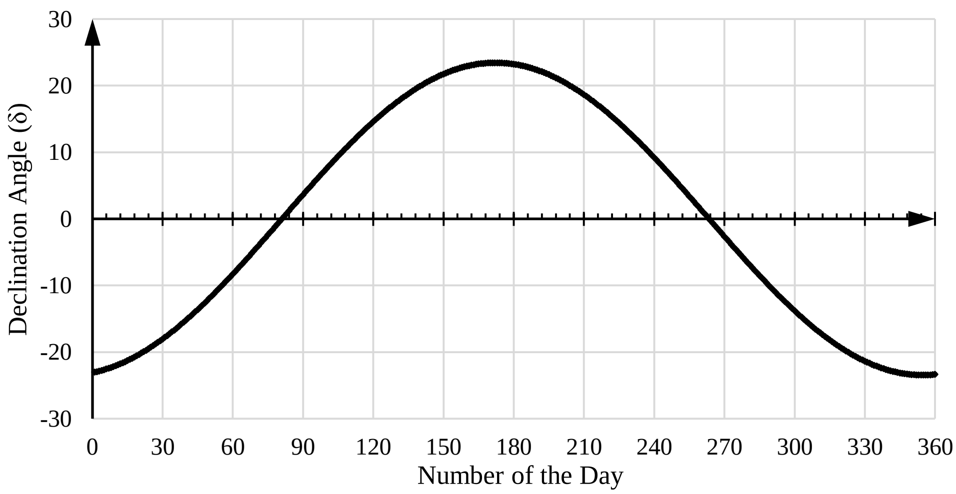

Figure 2.5 Time dependent fluctuation of declination angle

A couple of equations were found in order to calculate the incidence angle (θ) (Duffie & Beckman, 2013). Calculation of incidence angle (θ) is dependent to a certain day of a month which was given in Table 2.1. Incidence angle is an important parameter for a solar collector in terms of calculation of the optical efficiency. Some other solar angles, such as zenith angle, slope angle, declination angle, hour angle, surface azimuth angle and solar azimuth angle are required in calculation of the incidence angle.

Eq. (2.6) calculates the zenith angle (θ_z) using latitude (ϕ), declination angle (δ) and hour angle (ω).

$$\cos\theta_z = \cos\phi\cos\delta\cos\omega + \sin\phi\sin\delta \tag{2.6}$$

Eq. (2.7) shows relationship of solar azimuth angle with zenith angle (θ_z), latitude (ϕ) and declination angle (δ).

$$\gamma_s = \pm\cos^{-1}\left(\frac{\cos\theta_z\sin\phi - \sin\delta}{\sin\theta_z\cos\phi}\right) \tag{2.7}$$

Incidence angle (θ) can be calculated using Eq. (2.8) and it includes the following solar angles such as declination angle (δ), latitude (ϕ), slope angle (β), surface azimuth angle (γ) and hour angle (ω).

$$\begin{aligned}\cos\theta = {} & \sin\delta\sin\phi\cos\beta - \sin\delta\cos\phi\sin\beta\cos\gamma + \cos\delta\cos\phi\cos\beta\cos\omega \\ & + \cos\delta\sin\phi\sin\beta\cos\gamma\cos\omega + \cos\delta\sin\beta\sin\gamma\sin\omega\end{aligned} \tag{2.8}$$

Eq. (2.9) can be also used in calculation of the incidence angle (θ) as an alternative equation. It includes the effects of zenith angle (θ_z), slope angle (β), solar azimuth angle (γ_s) and surface azimuth angle (γ).

$$\cos\theta = \cos\theta_z\cos\beta + \sin\theta_z\sin\beta\cos\left(\gamma_s - \gamma\right) \tag{2.9}$$

However, utilizing coarsely the incidence angle in estimation of optical efficiency could not be adequate to trace the reflected rays. Because the incidence angle has to be divided into its components as transversal and longitudinal; so that, it will be able to yield the proper angle component in respect with the orientation of the surface. Figure 2.6 is a supportive approach in order to visualize three dimensional aspects of θ, θ_T and θ_L. Longitudinal and transversal angles were demonstrated in a prism system. Elements of the system is represented by colored rays; the collector surface by green, incident ray (from the sun) by red, longitudinal ray by yellow and transversal ray by blue. θ, θ_T, θ_L and γ_S represents incident angle, transversal angle, longitudinal angle and solar azimuth angle, respectively.

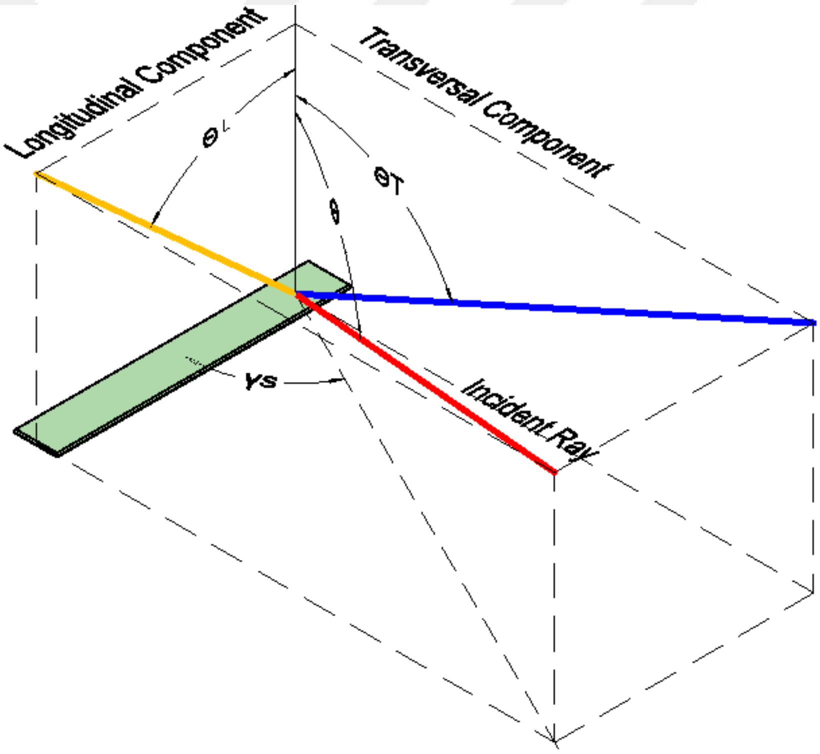

Figure 2.6 Demonstration of incidence angle's components in a rectangular prism

Transversal and longitudinal components can be calculated by the Eq. (2.10) and Eq. (2.11). It is vital to keep it in mind that solar azimuth angle is an essential parameter in the calculation of components in which an accurate result can be obtained. Angles are in degrees, not radians.

$$\theta_T = 90 - \tan^{-1}\left(\frac{\cos\theta}{\sin\theta\sin\gamma_s}\right) \tag{2.10}$$

$$\theta_L = 90 - \tan^{-1}\left(\frac{\cos\theta}{\cos\gamma_s\sin\theta}\right) \tag{2.11}$$

2.2 Stationary and Sun Tracking Solar Collectors

Solar collectors are instruments gathering solar irradiation. Amount of the collected solar irradiation depends on the material, direction and slope of the collector. Solar energy is absorbed and converted to useful heat by transferring to fluid. However, the maximum temperature that regular solar collectors can reach is limited. It is thought that concentration of solar energy can lead to higher temperatures. Solar collectors are divided as stationary and tracking collectors. Flat plate, evacuated tubes and compound parabolic collectors can be exemplified for stationary collectors. Parabolic trough, linear fresnel reflectors, parabolic dish and heliostat (central receiver) collectors are defined as sun tracking collecting systems and it is shown in Figure 2.7.

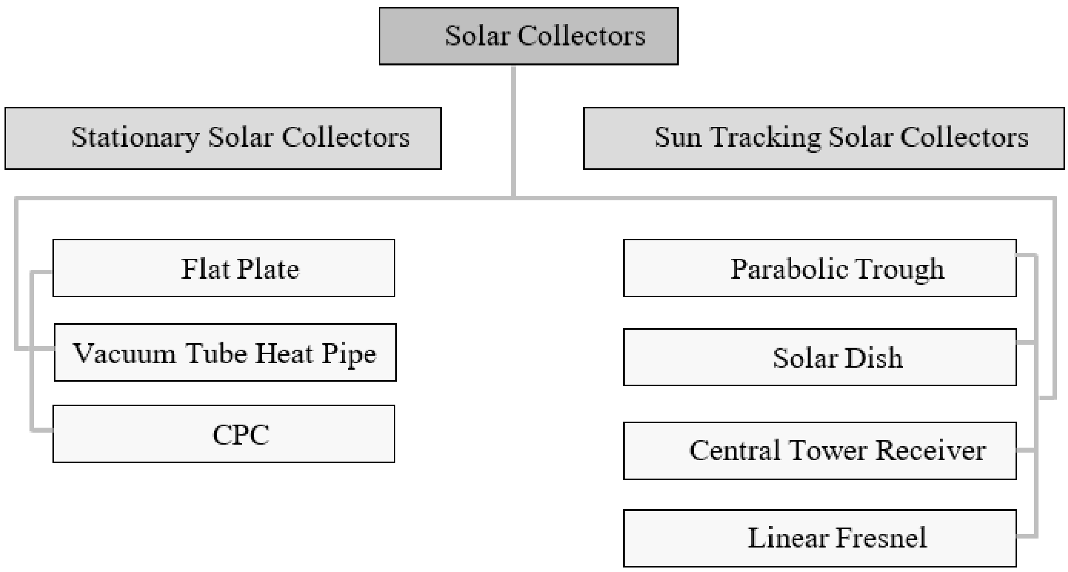

Figure 2.7 Classification of solar collectors

2.2.1 Stationary Solar Collectors

2.2.1.1 Flat Plate Solar Collector

Flat plate solar collectors are the most known and applied collector type around the world. It is basically consisted of collector case, absorber surface, capillary tube, insulation material and glass cover, which are illustrated in Figure 2.8. Collector case is insulated with foam, fiberglass or stone wool at the back and sides of the absorbing surface. Few sun rays are reflected from the glass cover, however most of them is transmitted to the absorbing surface. Flow tubes are mounted on the absorbing surface so that, absorbed solar energy is transferred to the working fluid in the tubes. Nevertheless, conduction and convection heat losses occur in the collector case.

Main objective of glass cover is to reduce convection heat losses from absorbing surface to the ambient and to protect it from rain and dust. The protective cover is selected glass which involves low Fe_2O_3; it has to transmit short wavelength rays and prevent long wavelength rays going out of the collector. This is why, solar transmittance of the glass cover should be high and on the contrary, the reflectance should be low.

Selection of absorbing surface material is performed according to the thermal conductivity of the material. Generally, aluminum, copper or steel is selected due to their high heat conduction properties. Steel is the cheapest material among them, however, it is not resistant to corrosion. For this reason, aluminum or copper is selected.

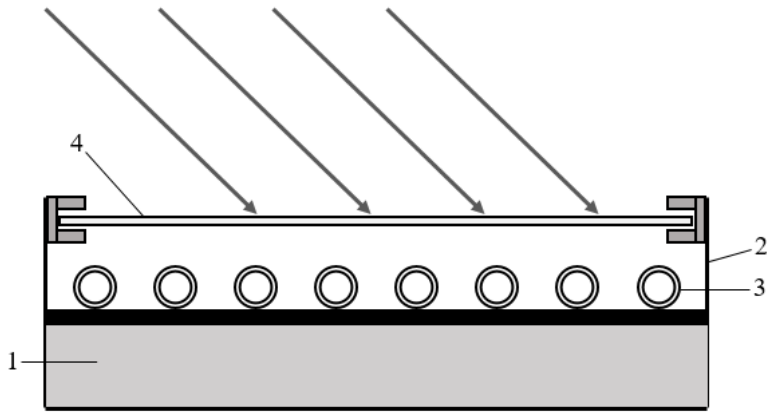

Figure 2.8 Cross section of flat plate solar collector; 1-insulation, 2-collector case, 3-flow tube, 4-glass cover

2.2.1.2 Evacuated Tube Heat Pipe Solar Collector

Vacuum tube or evacuated tube is consisted of two concentric borosilicate tubes whose medium between the tubes is evacuated, so that convective heat losses are considerably reduced. Outer surface of inner tube is covered with selective coating of Al-Cu/SS which allows higher absorption and lower emission. Borosilicate tubes have different sizes such as 47 mm outer diameter, 37 mm inner diameter and a thickness of 1.6 mm.

Tubes are vacuumed in high temperature environment and the bottom is sealed in dome form. Hence, thermal efficiency of vacuum tubes is much better than any other solar collector. Vacuum blocks the absorbed heat to get away from the selective coating. Most of the absorbed heat is transferred to the working fluid inside the inner tube. Number of vacuum tubes in a collector depends on the need of hot water. Sun rays are absorbed pretty much vertical during the day due to its circular form, so that sun rays are absorbed efficiently. Also, it is resistant to severe climate conditions.

However, evacuated tube heat pipes are also consisted of two concentric borosilicate glass tubes. Figure 2.9 illustrates that the evacuated tube heat pipe, in which traditional vacuum tube’s open end is closed (condenser) using a special dome-shaped geometry to be more resistant to axial loads. By means of created closed volume, an ethanol mixture is injected as heat transfer fluid.

Figure 2.9 Evacuated tube heat pipe (Sistem Tubular Online Catalogue, n.d.)

Selective coating on the surface of inner tube converts the solar energy to the heat and it is transferred to the fluid inside the tube. Heated fluid changes its phase to gas, and it rises to the dome-shaped condenser end which is plunged into the domestic water tank. By reason of outer surface of dome-shaped condenser is in contact with relatively colder domestic water, the heat transfer fluid in gas form inside the evacuated tube heat pipe is condensed on the inner surface of dome-shaped condenser. A commercial solar collector with evacuated tube heat pipe is illustrated in Figure 2.10.

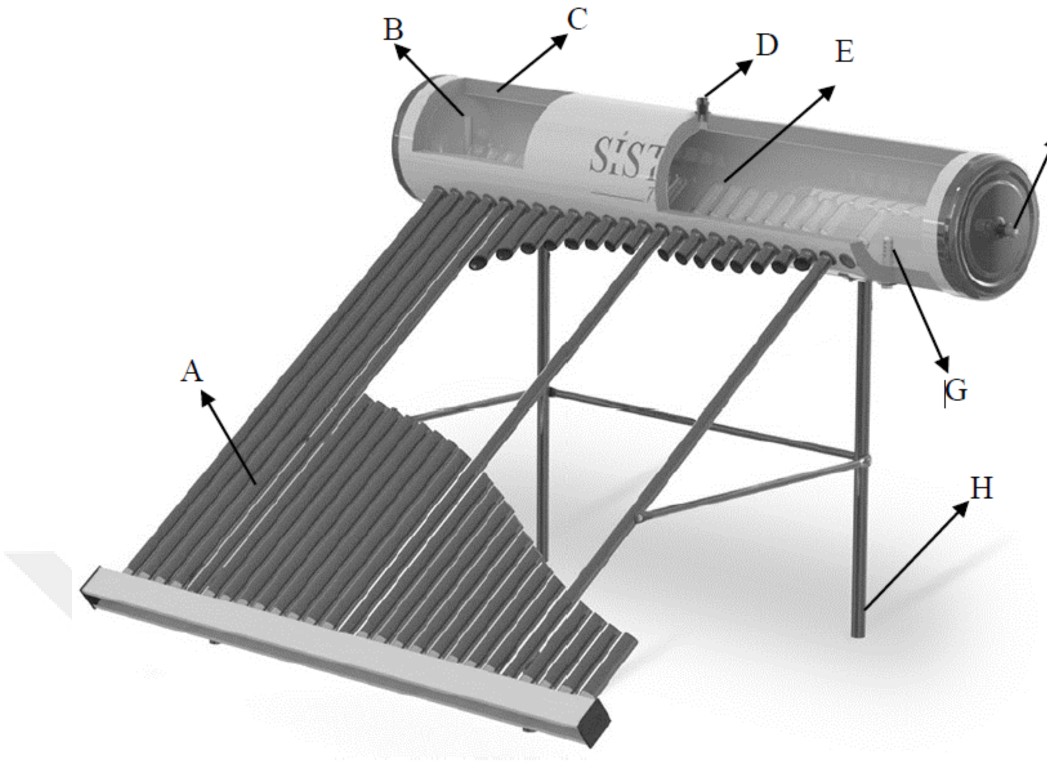

Figure 2.10 Solar collector with evacuated tube heat pipe. A- Evacuated tube heat pipe; B- Hot water outlet; C- Polyurethane foam; D- Air discharge valve; E- Heat pipe condenser; F- Temperature and pressure control valve; G- Cold water inlet; H- Supporter wireframe (Sistem Tubular Online Catalogue, n.d.)

2.2.1.3 Compound Parabolic Concentrator

Compound parabolic concentrator (CPC) is a non-tracking and stationary solar concentrator. It is consisted of an absorber and a reflector. Production and installation of CPC is cost effective and high efficient. Efficiency of the CPC depends on the absorber type and the working fluid. In Figure 2.11, a CPC collector is illustrated.

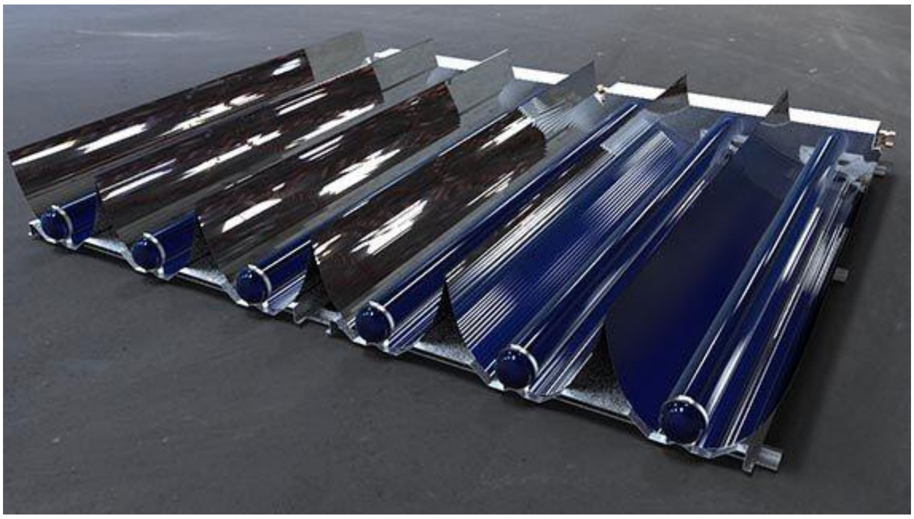

Figure 2.11 Collector of compound parabolic concentrator (Artic Solar, n.d.)

For air flowing applications, it is hard to reduce heat losses due to absorber surface, however, for domestic utilization such as water heating, heat losses are mostly reduced thanks to evacuation of vacuum tubes. Due to the special geometry of the reflectors, the CPC concentrates sun rays on its absorber in a significant time period. Cost of sun tracking system is passed over with the CPC applications.

2.2.2 Sun Tracking Solar Collectors

2.2.2.1 Parabolic Trough Collector

Parabolic trough collectors (PTC) are appropriate for obtaining high temperature working fluid and generating electricity. Their most popular installation areas are in deserts where cost of terrain is cheap and solar irradiation is high. Due to their high concentration ratio, production of superheated steam or hot fluid up to 400°C is possible. PTC’s make use of direct irradiation in which a sun tracking system is a must. That is why, PTC’s are generally mounted in the North-South alignment, so that sun tracking can be accomplished during the day, from East to the West.

Sun rays fall into aperture of parabola and are reflected to the focal point where absorber is mounted. In order to prevent convection losses and dust, a glass cover is applied over the absorber tube or receiver tube. Reflectors or mirrors which have high reflectance coefficient are most of the time preferred. However, the more reflectance, the more expensive reflector prices.

PTC is gaining popularity day by day so that private sector and universities interested in research, development and installation. In Figure 2.12 shows a PTC plant which was installed on the roof of Izmir Teknopark Innovation Center by Lucida Solar. It is located in the campus of Izmir Institute of Technology. The system provides industrial process heat with a temperature up to 210°C at 19 bar so that the innovation center is heated and cooled. As a result of two-axis tracking, it was observed that efficiency of the system is 37% greater than regular one-axis PTC plants (Lucida Solar, n.d.).

Figure 2.12 Parabolic trough collector plant in Izmir Teknopark (Lucida Solar, n.d.)

2.2.2.2 Linear Fresnel Concentrator

Linear fresnel concentrator (LFC) concentrates sun rays to a fixed absorber which is mounted above the reflector mirrors. Figure 2.13 shows that lots of linear mirrors are placed in different tilt angles on the ground and mirrors rotate depending on time so that one-axis tracking of sun is occurred. Hence, absorber heat losses have to be reduced in order to achieve higher efficiency (Taylor, Manikumar, & Arasu, 2014).

A tubular absorber is generally preferred; however flat absorber is to be determined in certain applications. In order to decrease the losses of reflected rays, a second reflector above the absorber is operated. Main reasons of lower optical efficiency are shape of reflectors, shading effects and the need for another reflector (Bellos, Tzivanidis, & Papadopoulos, 2018).

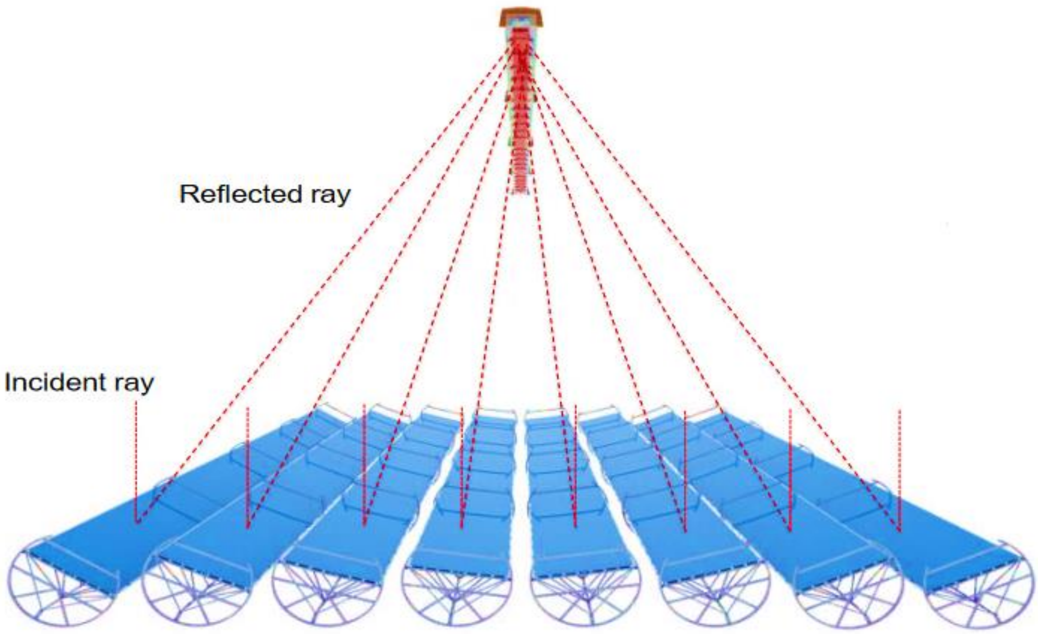

Figure 2.13 Linear fresnel concentrator (Bellos, Tzivanidis, & Papadopoulos, 2018)

2.2.2.3 Solar Dish Concentrator

Figure 2.14 represents a solar dish concentrator (SDC) which is a modular energy conversion system whose power ranges 5 kW to 25 kW. SDC's are equipped with heat engines, but mini gas turbines can also be utilized. Due to the modularity of SDC's, they are suitable for off grid applications and huge investments are not required. Direct irradiation is concentrated to its focal point in order to generate electricity. Concentrated sun rays are transferred to the heat engine and converted to mechanical energy. Mechanical energy drives the generator and then, electricity is generated. Because of focal point concentration, a two-axes sun tracking system is required. Focal point concentration provides much higher concentration ratios in comparison with line concentrating collectors. Possible peak temperature can get up to 750°C (Günther & Shahbazfar, 2011).

Figure 2.14 Solar dish concentrator (Günther & Shahbazfar, 2011)

2.2.2.4 Central Tower Receiver

Central tower receiver (CTR) is consisted of mirrors (heliostats) and a tower where mirrors track sun in two-axis. Sun rays are concentrated to the top of the tower in which concentrated solar irradiation is converted to useful heat. Water or molten salt can be utilized as working fluid in order to transfer heat. CTR can heat the fluid up to 800°C~900°C. After the fluid is heated, it is pumped to the turbine where it is attached to a generator. Then, electricity is generated. In addition, thermal storage can be a matter of concern, in case of generating electricity in the absence of sun and at night. Due to the costs, the popularity of commercial CTR is limited. It is shown in Figure 2.15 that a CTR is built in 2013 in the city of Mersin by Greenway CSP. The city is located on the Mediterranean coast of southern Anatolia where yearly high solar irradiation is occurred. The CTR's tower is as high as 50 m and 510 two-axis sun tracking heliostats concentrate solar irradiation. Its thermal power is of 4 MW and the plant has an operating temperature of 550°C at 55 bar (Greenway CSP Solar Tower, n.d.).

Figure 2.15 Greenway CSP central tower receiver in Mersin, Turkey (Greenway CSP Solar Tower, n.d.)

CHAPTER THREE
THE DESIGN AND THE OPTICAL ANALYSIS OF A COMPOUND PARABOLIC CONCENTRATOR

A compound parabolic concentrator was designed in Solidworks and the optical analysis was performed with the help of RayViz® software. Incident sun rays to the absorber tube was visualized so as to determine ray losses, design errors and path of reflectance. Implemented analysis was processed in another software, TracePro®, so that, values of absorbed irradiation would be displayed. After that, the optical efficiencies of various incident angles were combined with diameter, length and solar angles for obtaining a total optical efficiency of a day.

3.1 Basic Design of the CPC

The early design and optical performance study of CPC was made by Roland Winston (Winston, 1974). CPC is fundamentally consisted of two elements; reflector and absorber. The reflector is formed to obtain maximum number of incident rays which are directed to the absorber. However, absorber depends on the need for amount of useful heat and working fluid. Moreover, heat loss is a critical matter that has to be kept in mind for selecting the absorber. In the literature flat one-sided, fin, tubular, wedge, rectangular duct, oval and elliptical absorber types exist.

In Figure 3.1, a CPC structure, which consists of a reflector and an absorber is illustrated. Reflectors are located symmetrically with respect to the collector’s main axis and connected with the involute so that a uniform reflector structure is formed. Focal point of right parabola is positioned at the beginning of the left parabola and focal point of the left parabola is positioned at the beginning of the right parabola. This geometrical assembly allows sun rays, which come into the aperture at the acceptance half angle, to be collected on the focal points of two parabolas. However, when the sun rays are in the range of the acceptance half angle’s limits, they are collected at the different parts of the absorber.

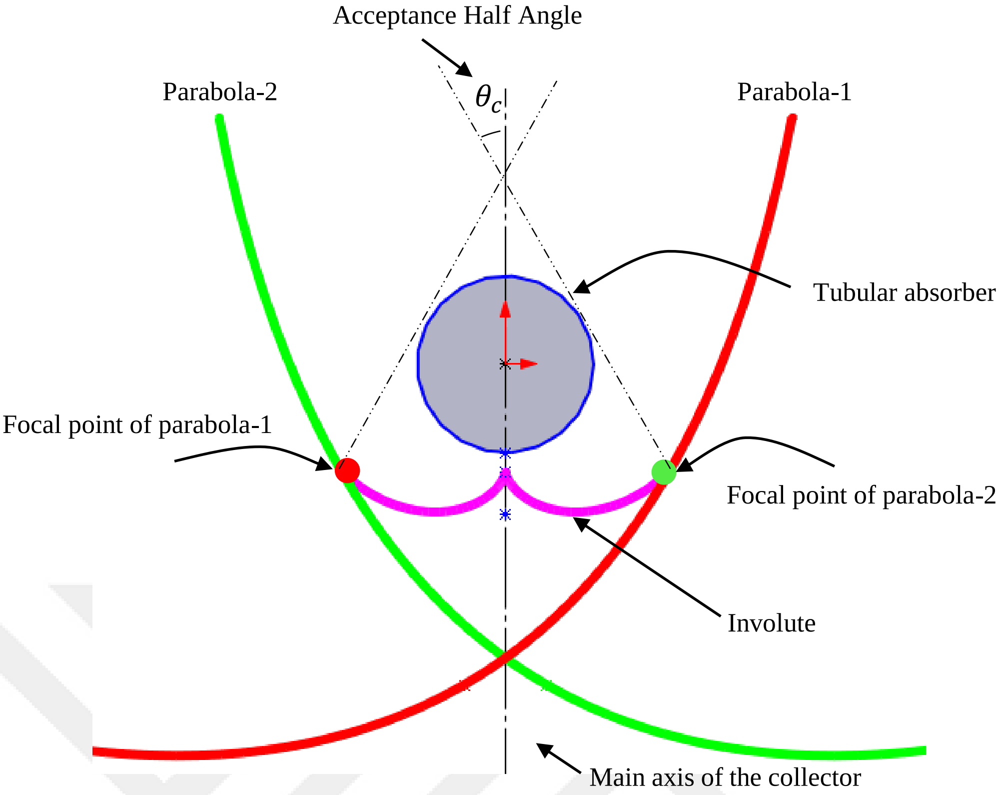

Figure 3.1 A tubular absorber, parabola, focal point and involute in a CPC drawing

3.2 Involute of the CPC

The involute of a circle is the pathway followed by a point on a straight line that rolls around a circle. Involute is generally utilized with CPC's which have tubular absorbers. Sun rays at different angles will mostly intercept with the tubular absorber surface after getting reflected. However, sun rays which are tangent to the tubular absorber is reflected back by the involute of the CPC (Shah, Srinivasan, & Murthy, 1990). The involute is defined in respect with the Cartesian coordinates shown in Figure 3.2. A tubular absorber which have a radius of R, an acceptance half-angle of θ_c, the width of ρ and a tangent line from the absorber to the curve is associated with the angle of θ. It is the angle between the radius to the bottom of the absorber and the radius to the point of tangency of T, and is represented by the following expressions for the both parts of the curve. The curve is composed by augmenting the θ in radians and calculating the coordinates of x and y (McIntire, 1979). The x and y axis of involute is defined in Eq. (3.1) and Eq. (3.2), respectively.

$$x = R \cdot sin\theta - \rho \cdot cos\theta \tag{3.1}$$

$$y = -R \cdot cos\theta - \rho \cdot sin\theta \tag{3.2}$$

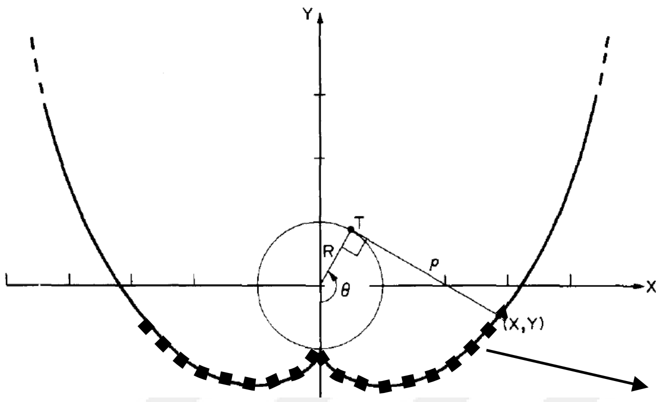

Figure 3.2 Schematic of the involute of a circle (McIntire, 1979)

3.3 Concentration Ratio of the CPC

Concentration ratio is affected with acceptance half angle which was shown in Figure 3.1. It is an important parameter for a collector, because it designates eventually the peak temperature that the CPC could reach. A collector is specified according to its CR if it is in high, mid or low concentration range. The concentration ratio, for a given acceptance half angle (θ_c), can be calculated by Eq. (3.3) (Rabl, 1976).

$$CR = \frac{1}{sin\theta_C} \tag{3.3}$$

Collectors with high CR are tower receiver, parabolic dish and linear fresnel concentrator and they are in need of direct irradiation. CPC is classified in low concentration range, because it is non-imaging and suitable for small scale applications. Direct and diffuse irradiation enters together to the aperture of the concentrator. In Table 3.1, a chart is defined in order to categorize concentrated solar power (CSP) systems according to their CR's. It can be seen that CR of CPC can get as high as 5 among other CSP systems. In accordance with other non-tracking solar collectors, CPC has a great advantage of CR due to its reflective modification.

Table 3.1 Concentration ratios of some solar collectors (Kalogirou, 2009)

Collector Type	Concentration Ratio
Flat plate collector	1
Vacuum tube collector	1
Compound parabolic concentrator	1 – 5
Linear fresnel concentrator	10 – 40
Parabolic trough concentrator	10 – 85
Parabolic dish concentrator	600 – 2000
Solar power tower	300 – 1500

3.4 Acceptance Angle of the CPC

Incoming sun rays are limited by the acceptance angle, so that, it is the greatest angle that sun rays are accepted. After reflections, incident sun rays which are in the range of acceptance angle, are gathered on the absorber. However, pathway of incoming rays may change depending on time. Once the incidence angle of incoming rays is bigger than the acceptance angle, they cannot intercept with the absorber, they are directly reflected outward of the collector. For larger acceptance angles, seasonal adjustment, on the other hand, for smaller acceptance angles, a continuous sun tracking is a must (Tiwari & Shyam, 2016). Acceptance angle (θ_A) is the sum of two-acceptance half angles ($2\theta_c$). It is apparent in Figure 3.3 that sun rays having incidence angle (θ_i) smaller than (Figure 3.3 a) the acceptance half angle (θ_c) can be collected at the absorber, however, it is not possible for sun rays (Figure 3.3 b) having incidence angle more than acceptance half angle.

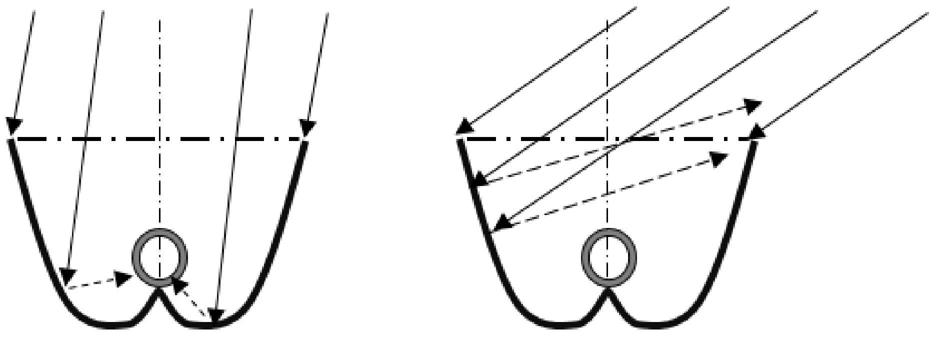

Figure 3.3 Incident sun rays in respect with the acceptance angle

The need for sun tracking system will be irrelevant in broader acceptance angles, in which, a position update is not required. Small acceptance angled concentrators are a matter of high CR. Smaller angles claim flawless and more expensive sun tracking systems, while wider angles result in small CR's and lower working temperatures. Namely, all of the sun rays must intercept with the absorber, in the range of $\theta<\theta_{max}$. All rays which are caught on the absorber are within the acceptance angle and any rays out of the range of the acceptance angle are not caught to the absorber. It can be clearly seen from Table 3.2 that a collector with low acceptance half-angle requires tilt adjustments at regular intervals. In order to invalidate annual tilt adjustments, an acceptance half angle bigger than 19.5° is required (Rabl, 1976).

Table 3.2 Adjustment of collector tilt (Rabl, 1976)

Acceptance Half Angle (Ideal Concentration Ratio)	Collection Time Average Over Year (hours per day)	Number of Adjustment per Year	Shortest Period Without Adjustment
19.5° (3.0)	9.22	2	180 days
14° (4.13)	8.76	4	35 days
11° (5.24)	8.60	6	35 days
9° (6.39)	8.38	10	24 days
8° (7.19)	8.22	14	16 days
7° (8.21)	8.04	20	13 days
6.5° (8.83)	7.96	26	9 days
6° (9.57)	7.78	80	1 day
5.5° (10.43)	7.60	84	1 day

3.5 Truncation of the CPC

CPC's are able to reach its maximum potential in terms of concentration ratio for a given acceptance half-angle, and in accordance with the energy necessity, a variety of CPC structures exist. The reflector's upper surface of a CPC is practically vertical to the aperture area, thus, the upper reflector contributes less to the concentration of rays. A CPC is commonly truncated more or less about half of its full height in order to increase the ability of ray incidence, save reflector material and reduce the production cost. Figure 3.4 represents the association of concentration and truncation, in which the concentration ratio decreases roughly 1.66 to 1.51 if the reflector is truncated by 60% of its full height. As it can be seen, truncation widens the ability of gathering sun rays in numerous angles, even though; rays, which are out of the acceptance angle, can be collected. (Carvalho, Collares-Pereira, Gordon, & Rabl, 1985).

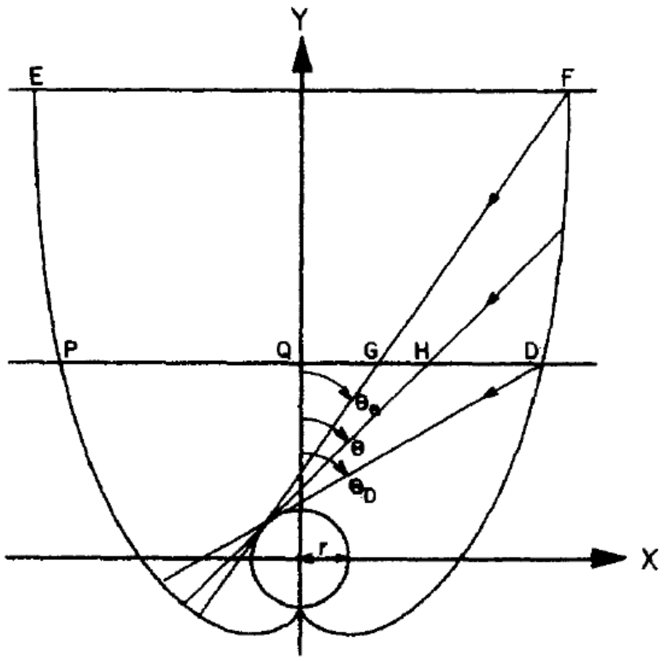

Figure 3.4 CPC with acceptance half-angle of θ_A and tubular absorber of radius *r*. Aperture of untruncated CPC: *EF;* aperture of truncated CPC: *PD* (Carvalho, Collares-Pereira, Gordon, & Rabl, 1985)

3.6 Different Absorber Types of the CPC

There are many types of CPC depending on the absorber type. Figure 3.5 illustrates a couple of CPC with different absorber type, such as (a) flat one-sided, (b) fin, (c) tubular, wedge, rectangular duct, oval and elliptical absorber types exist, however, (d) tubular, flat plate, and rectangular duct are the most popular types. A CPC is generally named after its form of absorber. Absorber type is chosen by on the amount of required heat and working fluid. In air heating applications, a rectangular duct or flat plate absorber with enhanced surface is generally preferred in order to defeat high heat resistance of air. On the contrary, tubular absorber with vacuum is utilized to minimize thermal losses in terms of water heating or steam generation. It is vital to emphasize that most of the studies and experiments have been developed over the CPC with tubular absorber.

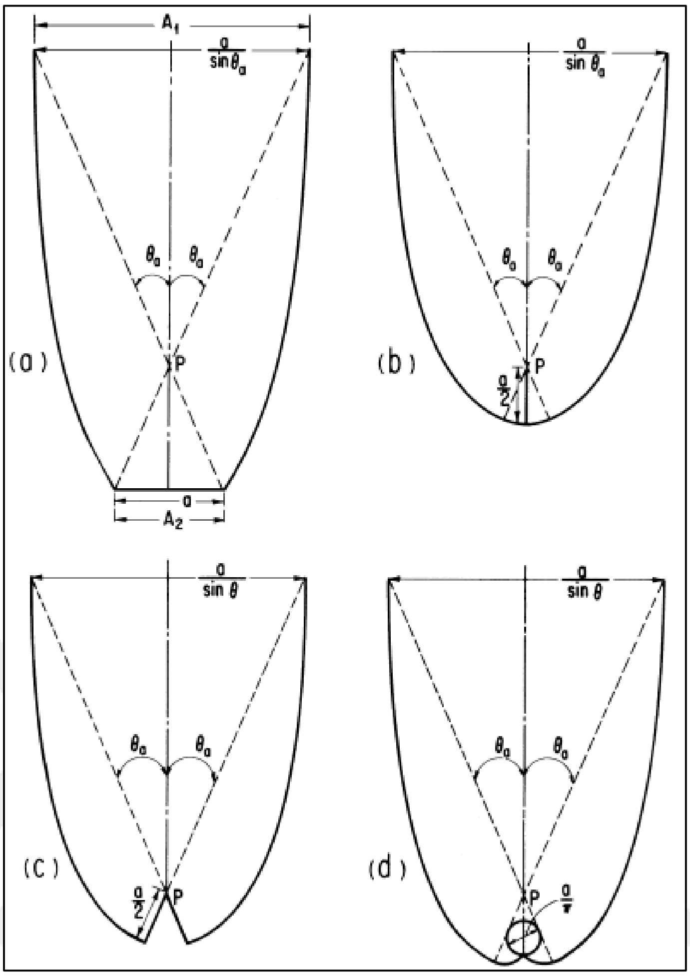

Figure 3.5 Different configurations of the CPC (Rabl, O'Gallagher, & Winston, 1980)

3.7 Design of a Compound Parabolic Concentrator

A CPC can be designed in a number of 2D or 3D CAD softwares, nevertheless, Solidworks was preferred for its simplicity and availability. A 2D CPC is drawn and it is converted to 3D by giving it a thin wall thickness. The drawing has to be totally defined, otherwise, software will show errors and 3D model cannot be created. That is why a thorough study has to be conducted.

The diameter of the absorber is required in order to begin the drawing. In the study, a vacuum tube with a diameter of 47 mm – outer tube and 37 mm – inner tube was used. Figure 3.6 shows that main axes are drawn by center line, so that the drawing can start at the center of the circle. Absorber is the outer surface of inner tube so that, 37 mm diameter circle was drawn, an acceptance half angle of 30° was applied and 30° axes are tangent to the circle. In application, most popular vacuum tube diameters are (inner/outer) 37/47 mm and 47/58 mm. Implementing one seasonal adjustment requires 30° acceptance half angle for Izmir, Turkey.

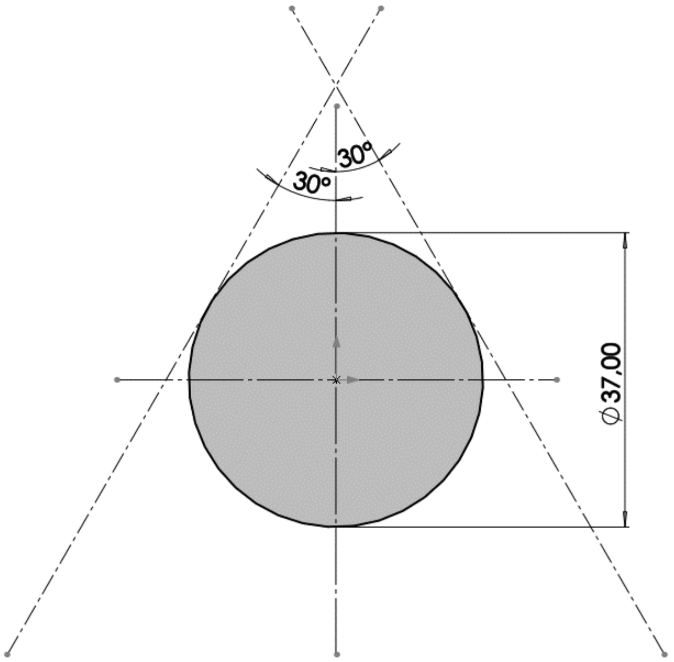

Figure 3.6 First step of the design of the CPC

After the first step, a line which is 5 mm away from the bottom of the circle is drawn in order to specify the 47 mm – outer tube. Then, a parabola has to be drawn. A parabola is the sum of equidistant points to the focus from a directrix. Hence, sun rays hitting the parabola will be collected at the focus. There are two parabolas in a CPC, consequently two foci exist and the circle is positioned between the foci. In Figure 3.7, point A is the focus of the parabola and the lines of $\overline{AB}$ and $\overline{BC}$ are equal to each other. $\overline{AD}$ is the focal length and point D is the bottom of the parabola. $\overline{AK}$ & $\overline{KC}$ and $\overline{KC}$ & $\overline{CB}$ lines have to be vertical to each other, in this case, $\widehat{BCK}$ is 90°. As it is shown in Figure 3.6, a parabola tilted 30° from the vertical centerline can be easily drawn in the following steps.

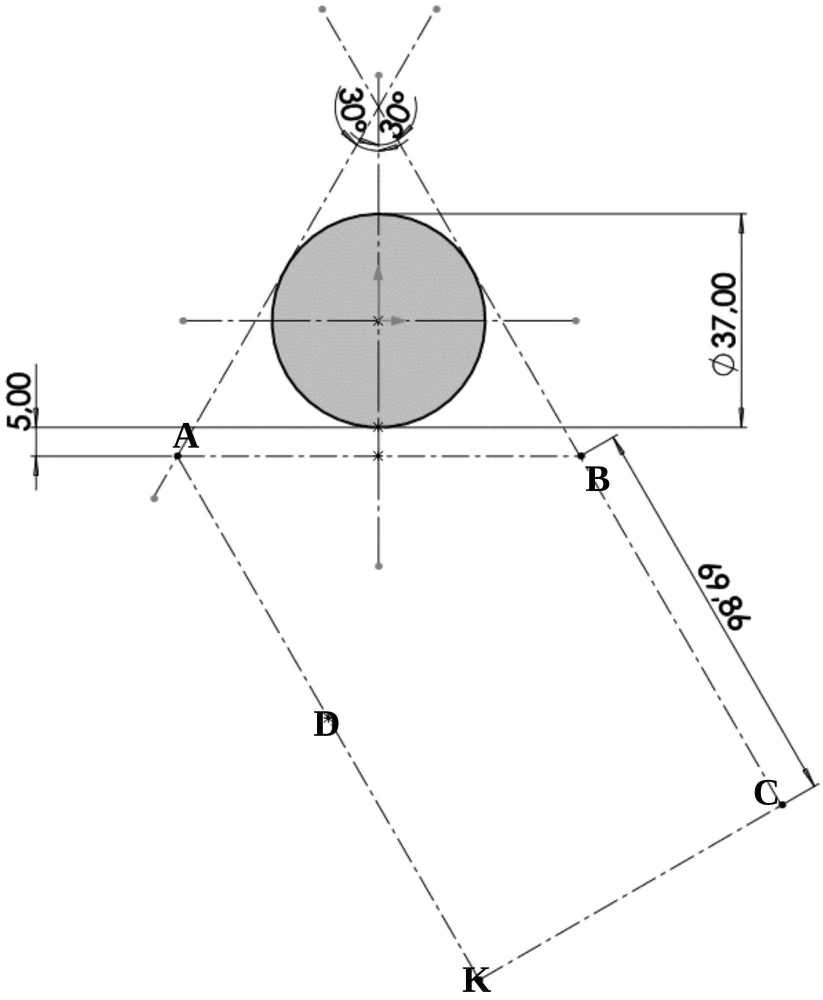

Figure 3.7 Preparation to draw parabola

In Figure 3.8, a full parabola was drawn. In design process, a full parabola always has to be drawn, then an accurate truncation can be applied. Parabola is drawn until it is perpendicular to horizontal surface and it is intersected with 30° axis line at this point. The left part of the parabola can be drawn by mirror command.

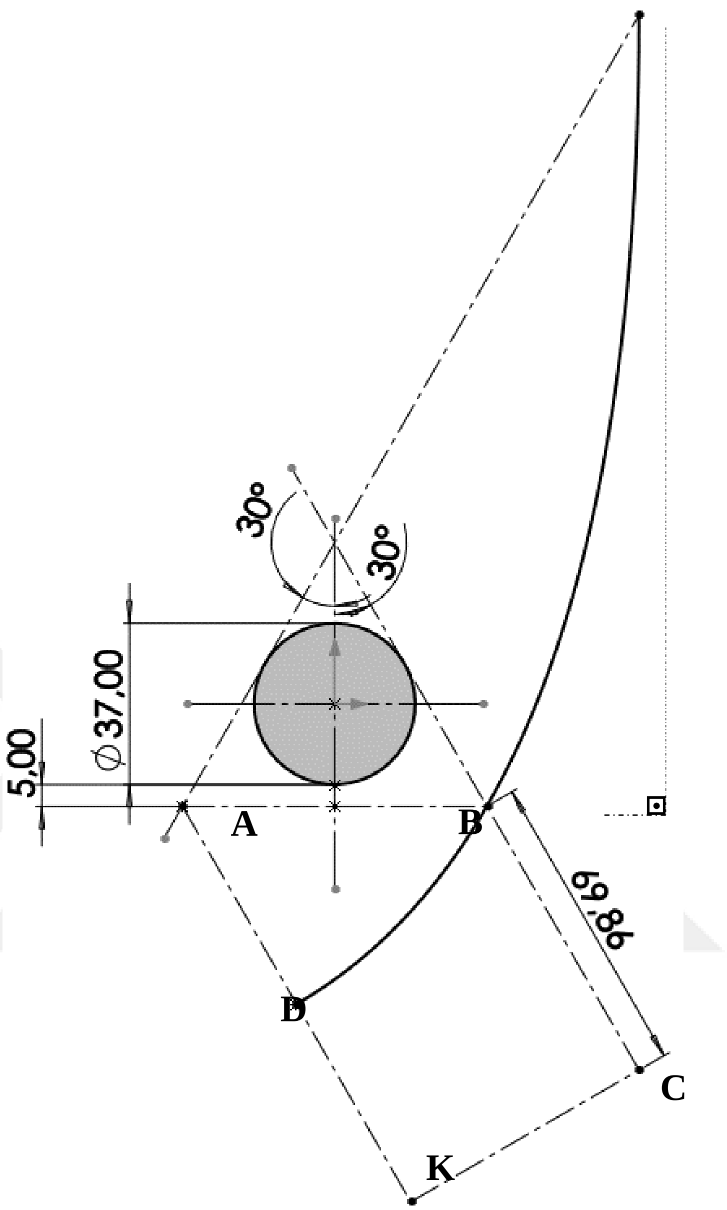

Figure 3.8 Drawing of the full parabola

Figure 3.9 shows that a CPC with tubular absorber requires an involute reflector which reflects sun rays to the bottom of the tubular absorber. Involute is required in case of tubular absorber. It is drawn with equation driven curve command by setting it to parametric equation type (Eq. (3.1) and Eq. (3.2)). After the involute is drawn, it has to be adjusted to coincide with the point B. After that, it can be mirrored to the other side. The most important point of drawing the involute and the parabolas are all the intersections must be coinciding, otherwise software will fail to extrude the 2D model.

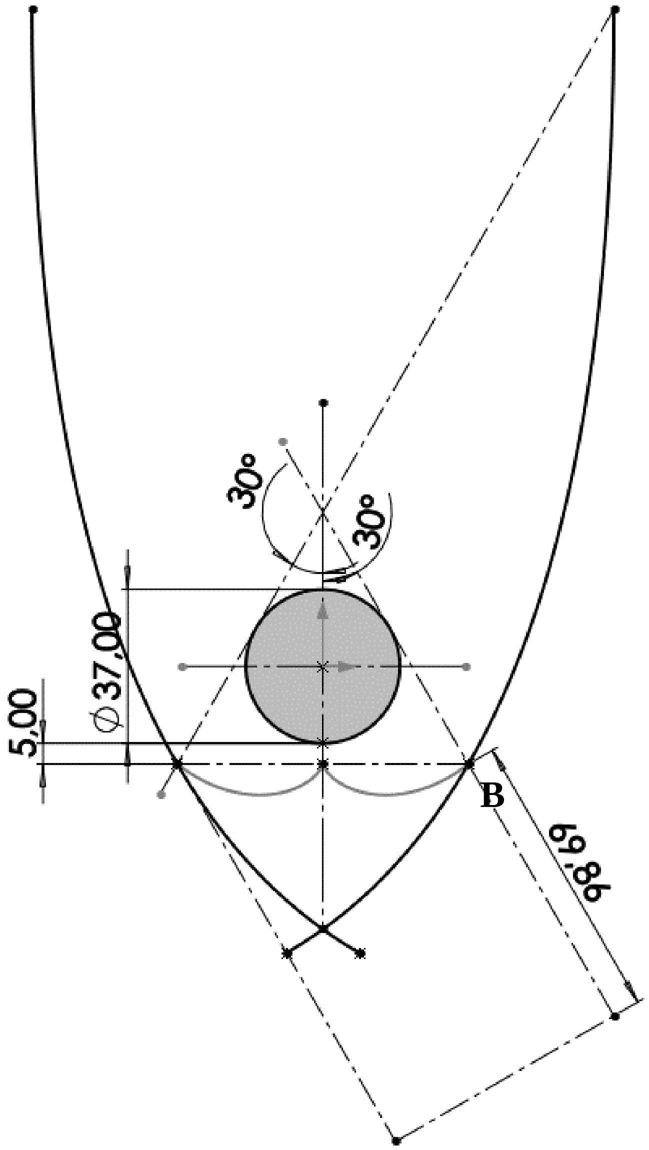

Figure 3.9 Full CPC with involute

Eq. (3.1) and Eq. (3.2) is used in Solidworks which are for drawing the involute. If the created involute is long, it can be trimmed. Figure 3.10 shows an axial truncated CPC with tubular absorber.

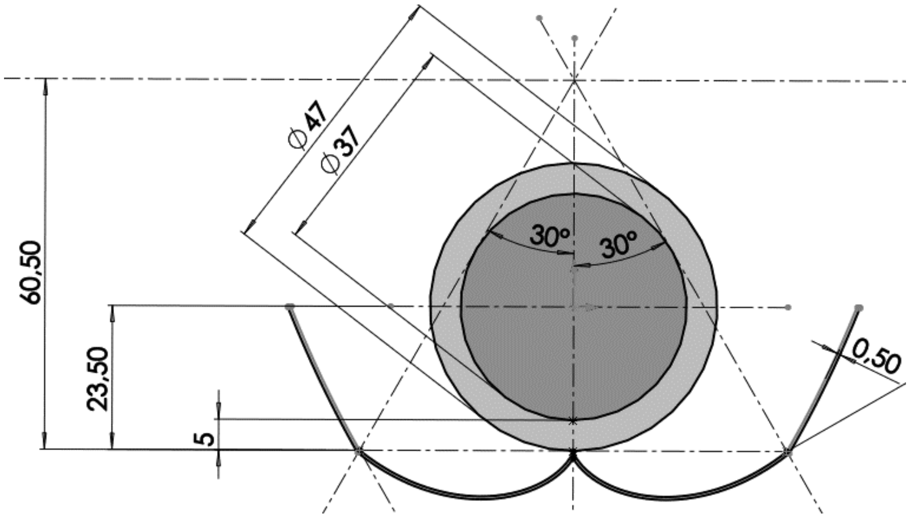

Figure 3.10 Truncated and offsetted CPC for creating 3D model

Yet, the CPC height must be shortened. In fabrication, shorter CPC heights are preferred due to manufacture and material cost. Even though, minimized CPC heights are preferred up to 3 cm. Thus, truncation is a must in the design and the production of the CPC. In this design, 87% of the parabola height is truncated, then the leftover part was offset 2 mm for 3D extrusion; the 3D reflector of CPC is shown in Figure 3.11. Length of the CPC is limited with the tubular absorber's length, in this case, it is 1800 mm. The designed CPC with dimensions is illustrated in Figure 3.11.

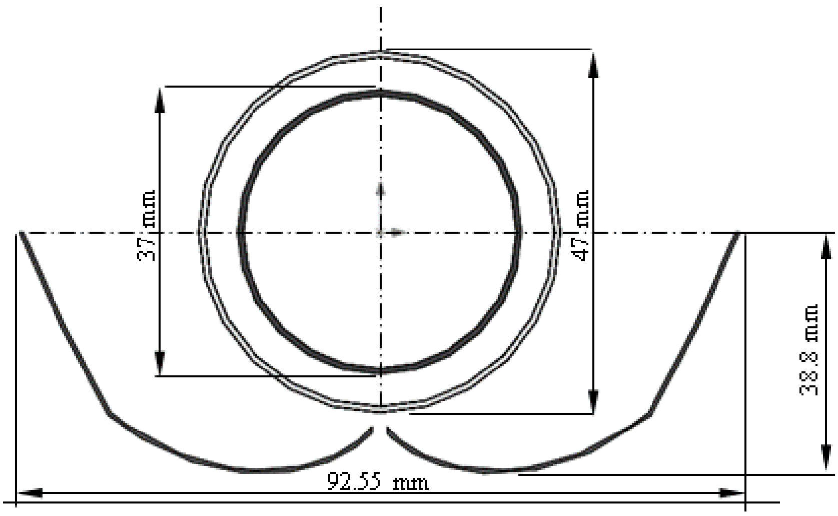

Figure 3.11 Front view of CPC and dimensions

3.8 Optical Analysis of a Compound Parabolic Concentrator

Optical analysis helps to detect mistakes, impurities and imperfect surfaces by applying virtual rays onto a surface and shows reflection directions. Reflected rays are directed to an absorber, in other words concentration occurs. After that, the rate of collected energy in the absorber can be revealed by the software and an optical efficiency value is obtained. RayViz, an add-in for SolidWorks, is used for optical analysis'. 3D modelled CPC with vacuum tube was analyzed in RayViz step by step as it is explained in the following.

Figure 3.12 shows a CPC with a virtual ray source. A ray source has to be created in order to dissipate rays to the aperture area of the concentrator. The ray source is required to have dimensions of CPC's aperture width and length so that all of the rays can be directed to the aperture. In SolidWorks, a rectangle is drawn and extruded; extrusion thickness does not matter. Then, ray tracing is accomplished in *Assembly*, by combining the ray source on the top of the CPC. The ray source and the upper plane of CPC must fit from both ends and sides, so that ray loss cannot take place.

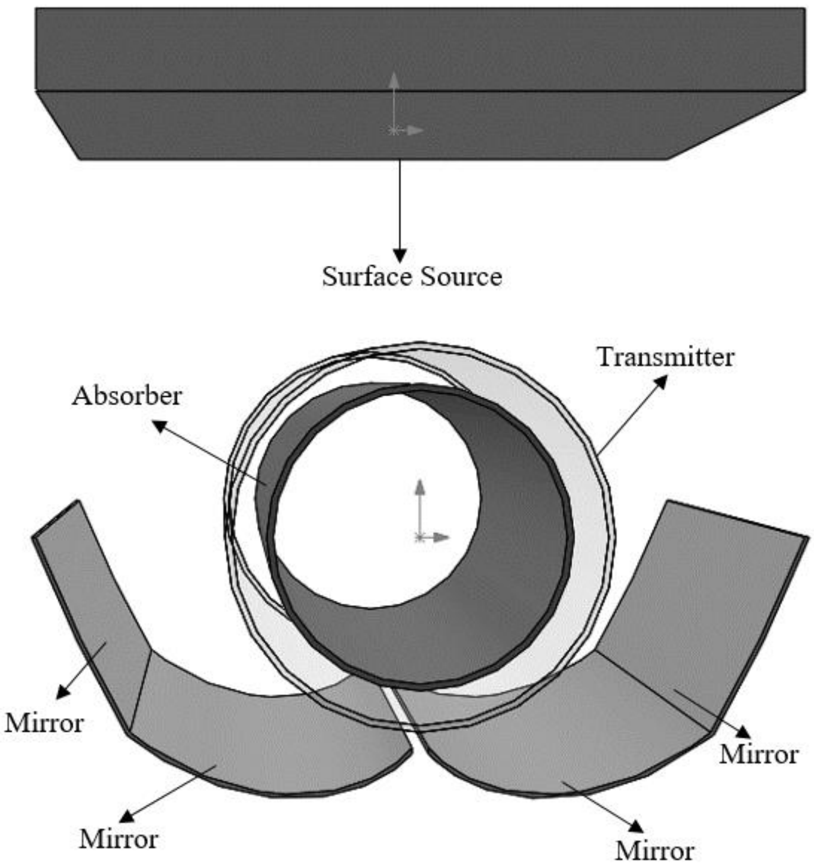

Figure 3.12 Perspective view of CPC with identified surfaces

Surfaces of CPC must be defined as reflector, transmitter and absorber. In the add-in, it is possible to select a variety of commercial materials or coatings. It is vital to emphasize that information about the coefficients of reflectance, absorptance and transmittance would be correct only by applying to the manufacturer of the material. After the model was created, optical properties of the surfaces were defined. The coefficients of reflectivity (ρ), transmissivity (τ) and absorptivity (α) were taken as 0.80, 0.90 and 0.925, respectively. The coefficients were obtained from the manufacturer of vacuum tube so that a consistent comparison can be made easily in the experiments.

Surface source is modified as in following; emission type - *Irradiance,* units - *Radiometric,* irradiance - *1 W/m^2*, minimum rays - *100,* total rays - *250,* angular distance - *Normal to Surface* and rays - *All Rays.* The more "total rays" are input – e.g., 1000 rays, the more accurate results are obtained. RayViz was executed between

0° to 60° with an increment of 15° incident angle and the ray paths were given in Figure 3.13, 3.14, 3.15, 3.16 and 3.17.

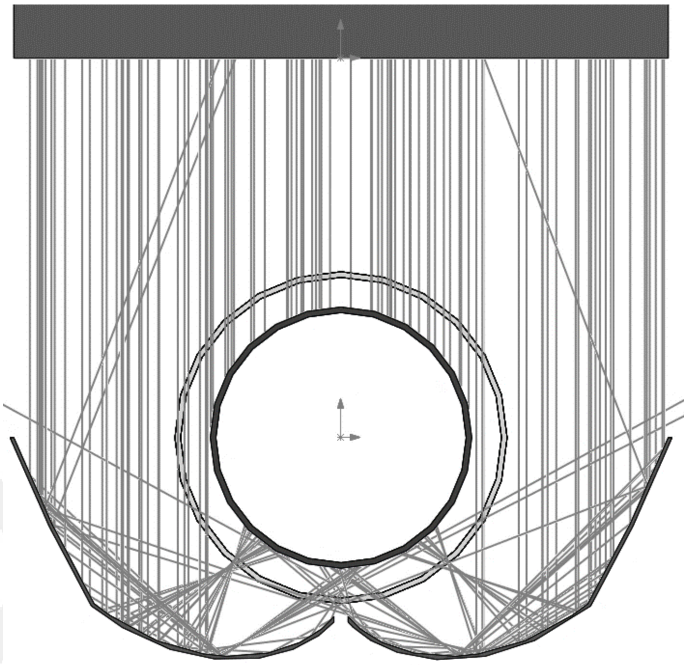

Figure 3.13 Ray paths for incident angle of 0°

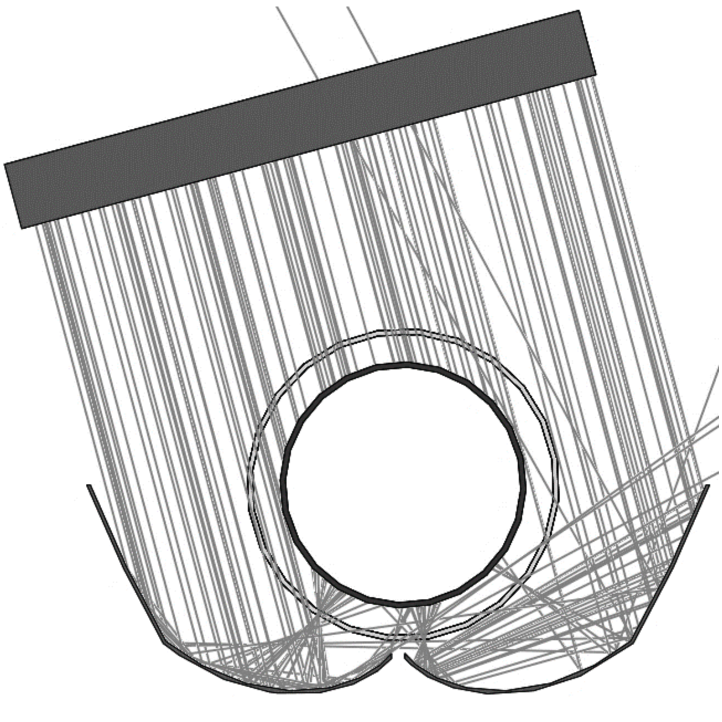

Figure 3.14 Ray paths for incident angle of 15°

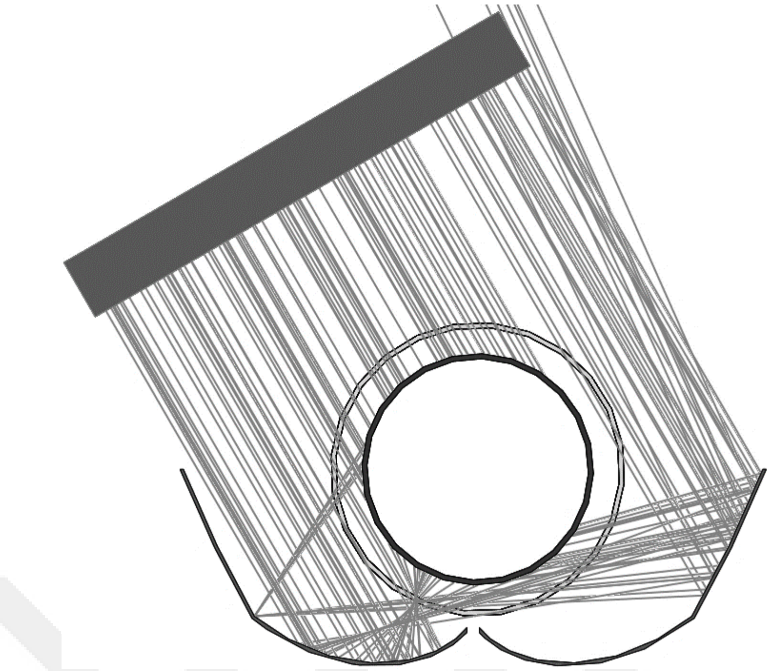

Figure 3.15 Ray paths for incident angle of 30°

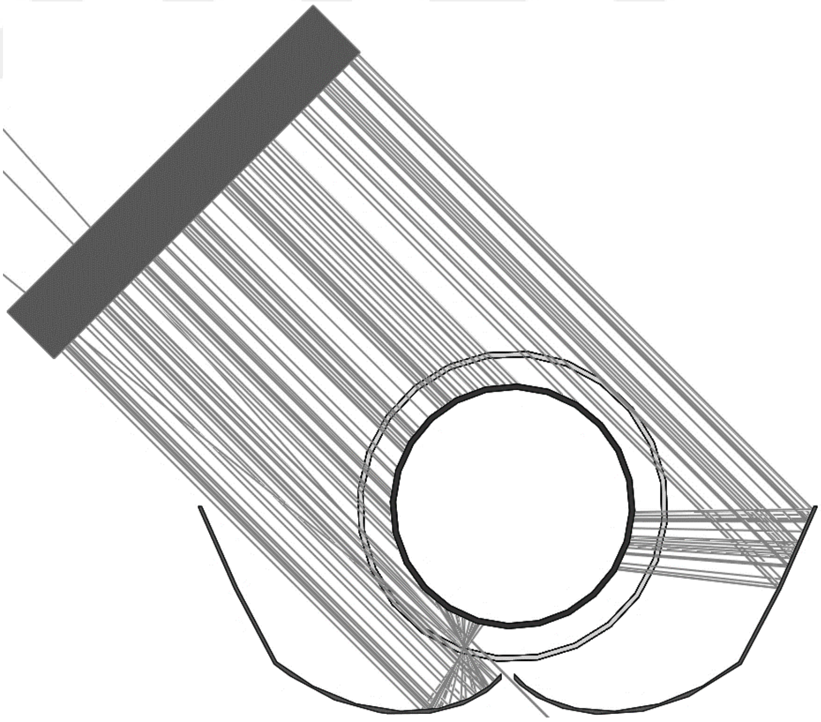

Figure 3.16 Ray paths for incident angle of 45°

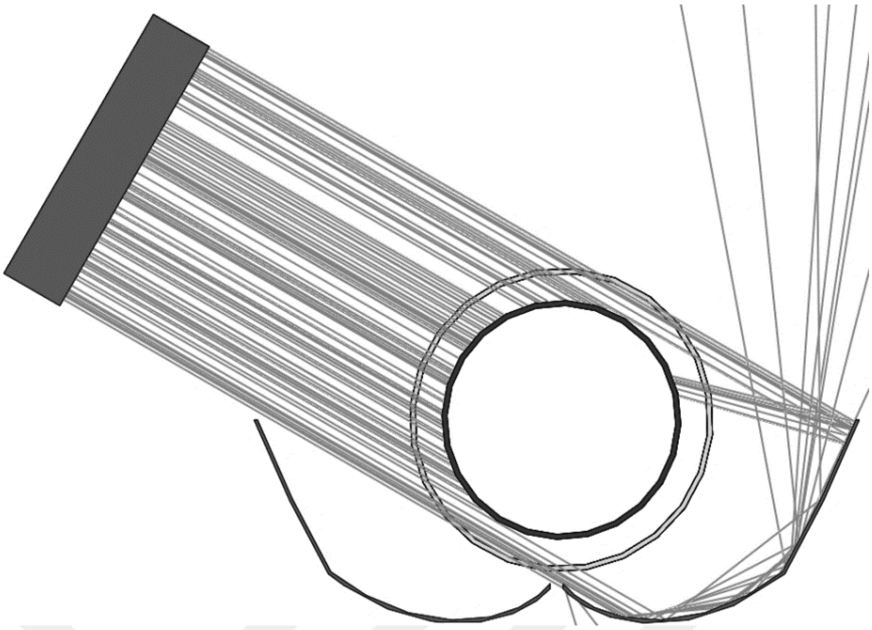

Figure 3.17 Ray paths for incident angle of 60°

3.9 Calculation of the Optical Efficiency

The optical efficiency is a fundamental parameter in order to estimate more accurate the total collected energy by a solar system. In the calculation of a system's optical efficiency, optical specifications of the system's elements such as, absorptance, transmittance and reflectance – has to be known. Besides, there are two variables (solar irradiance and transversal incidence angle) which depend on time. Solar irradiance can be obtained by some certain data providers such as Photovoltaic Geographical Information System (PVGIS) or the irradiation can be recorded by a pyranometer in a period of time. After that, the calculations have to be made for incidence angle by Eq. (2.8) and Eq. (2.9), its components by Eq. (2.10) and Eq. (2.11). Then, incident angle has to be divided into its components as transversal and longitudinal which were illustrated in Figure 2.6.

RayViz can only be utilized in order to see design faults for a geometry, numerical results such as optical efficiency or flux distribution can not be observed. There is another software called TracePro for the numerical results. The file in RayViz is saved as .oml file so that TracePro can read the created and ray traced file.

A model can be also created in TracePro, but SolidWorks is much more user-friend software. In TracePro, it is possible to define new materials and coatings to the surfaces or just coefficients can be assigned. TracePro was executed for a range of angles between 5° to 90° with an increment of 5°. A minimum angle increment is preferred because the small steps will reveal a pure optical efficiency.

Optical efficiency values were obtained by TracePro software and they are given in Figure 3.18. As it is seen, an average optical efficiency of 70.32% was revealed due to the CPC design. CPC's reflector height is a vital parameter on optical efficiency. Down to a specific height, it can be tolerated in terms of optical efficiency. The more important point is that the optical efficiency in the morning and afternoon is above than the noon. A high reflector height will not let the morning and afternoon efficiencies to be higher than the noon. However, solar irradiance is considerable low in the morning and afternoon rather than the noon. The incidence angle is the same at symmetrical hours according to the solar noon. In low solar irradiation, a high optical efficiency will contribute less to the total energy gain.

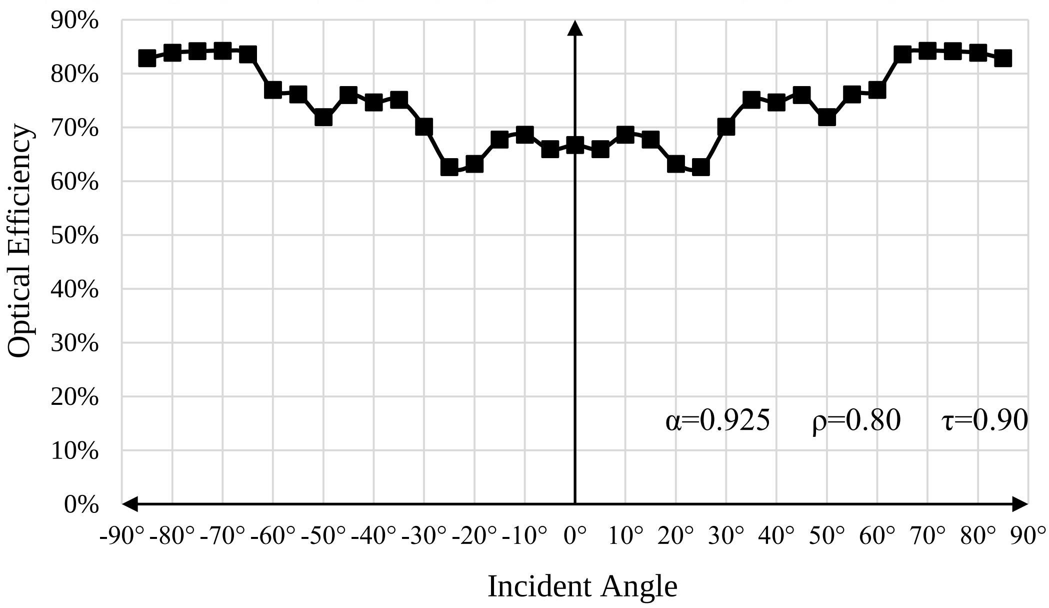

Figure 3.18 Optical efficiency of designed CPC depending on incident angle

3.10 Determination of Total Energy Gain and Thermal Efficiency

Total solar energy, $\dot{E}_{solar}$ (W), depends on the global irradiation (W/m^2), I_{irr} , and the aperture area of CPC (m^2), $A_{aperture}$ as in Eq. (3.4).

$$\dot{E}_{solar} = I_{irr} \cdot A_{aperture} \tag{3.4}$$

Total energy gain on the absorber surface, $\dot{Q}_{abs}$ (W), depends on the optical efficiency of transversal component of incident angle, $\eta_{opt,\theta}$ as in Eq. (3.5).

$$\dot{Q}_{abs} = \eta_{opt,\theta} \cdot \dot{E}_{solar} \tag{3.5}$$

$\dot{Q}_{loss}$ is the total energy loss from the absorber tube (W); depends on the coefficient of heat loss, $U_{overall}$, absorber area A_{abs}, the temperature of absorber surface, T_{abs}, and the ambient temperature, $T_{ambient}$, as in Eq. (3.6).

$$\dot{Q}_{loss} = \dot{U}_{overall} \cdot A_{abs} \cdot (T_{abs} - T_{ambient}) \tag{3.6}$$

$\dot{Q}_{flow}$ is the useful heat transferred to the fluid (W) as in Eq. (3.7).

$$\dot{Q}_{flow} = \dot{Q}_{abs} - \dot{Q}_{loss} \tag{3.7}$$

η_{th} is the thermal efficiency of CPC as in Eq. (3.8).

$$\eta_{th} = \frac{\dot{Q}_{flow}}{\dot{E}_{solar}} \tag{3.8}$$

In order to calculate daily average thermal efficiency in Eq. (3.8), it has to be integrated for the working hours as in Eq. (3.9).

$$\eta_{th,day} = \frac{\int_{day} \dot{Q}_{flow} \cdot dt}{\int_{day} \dot{E}_{solar} \cdot dt} \tag{3.9}$$

CHAPTER FOUR
EXPERIMENTAL RESULTS OF COMPOUND PARABOLIC CONCENTRATOR WITH EVACUATED TUBE HEAT PIPES

An optical analysis was conducted for a single CPC with evacuated heat pipe. According to the results, the model is accepted to build a CPC with seven evacuated tube heat pipes. After the design and virtual assembly of the collector in SolidWorks, the solar collector's chassis, manifold and CPC ribs were manufactured. After the body of the collector is assembled, the evacuated tube heat pipes were placed in the collector. The collector was located and tested in Tınaztepe Campus of Dokuz Eylül University, in Izmir.

4.1 Preparation of the Experimental CPC

The CPC includes evacuated tube heat pipes surrounded with anodized aluminum reflectors which were assembled together with CPC ribs. CPC rib is a special design to ease and to reduce manufacturing cost of the collector. In current CPC reflector manufacturing, roll forming is applied to sheet metal in which long strips of sheet metal are bended through the rollers and it is shaped to a specified geometry. This process allows sheet metal's parabolic shape to be protected for a long time. Although, roll-forming machines require quite high initial investment cost. Our new design lets the manufacturer to produce the reflector of the CPC without roll forming. As it is shown in Figure 4.1, CPC rib has the same parabolic form that the reflector has. Reflector is slipped through the rib, because the rib has a proper gap for reflector in which the parabolic form is protected.

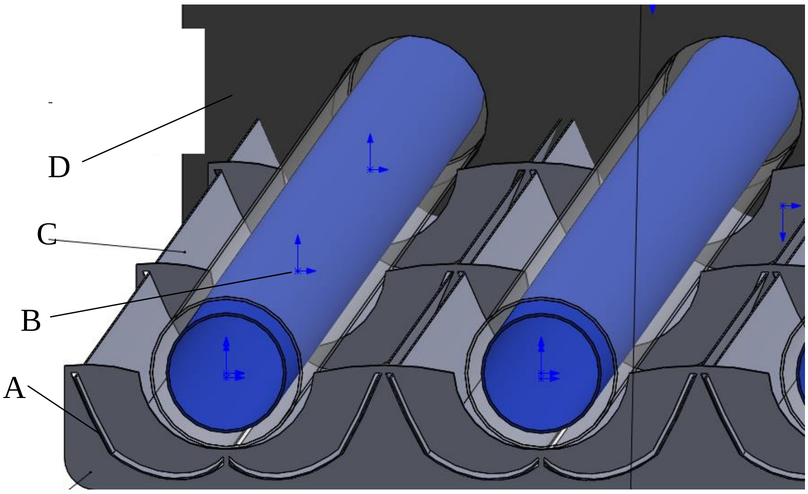

Figure 4.1 Perspective view of virtual assembly of the collector with CPC ribs, reflectors, evacuated tube heat pipes and manifold (A: CPC rib; B: evacuated tube heat pipe; C: reflector; D: manifold)

In this CPC prototype, three CPC ribs used to keep the parabolic form of the reflector. It is important to indicate that slipping the sheet metal through the CPC rib can create scratches on the reflector. A broad gap in the rib will not let the reflector to keep the parabolic form. That is why; a proper rib gap width is required. In the experiment, 2 mm gap was good enough for a thickness of 1 mm sheet metal.

As it is seen in Figure 4.1, involute's peak and tubular absorber fit tangential; however, a full involute wing length will cause an axial run-out in terms of CPC rib utilization. Therefore, a modification to involute's peak was developed in order to reduce the axial run-out. Optical analysis is carried out due to perfect design and a run-out is not taken into account. After the production, results of the solar experiment will be misled owing to run-out. Peak part was truncated symmetrically according to the vertical axis. The new modification of the CPC rib was designed so that the peak is as close as to the tubular absorber which is demonstrated in Figure 4.2. The final design which is used in the collector is given in Figure 4.3.

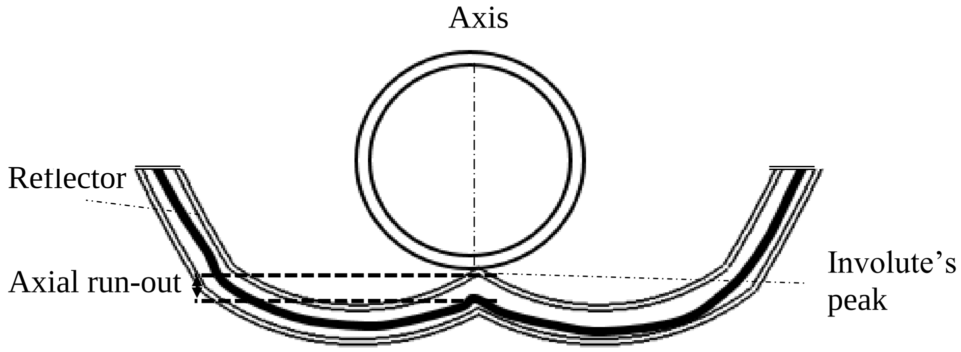

Figure 4.2 Axial run-out of reflector and absorber in terms of collector rib use

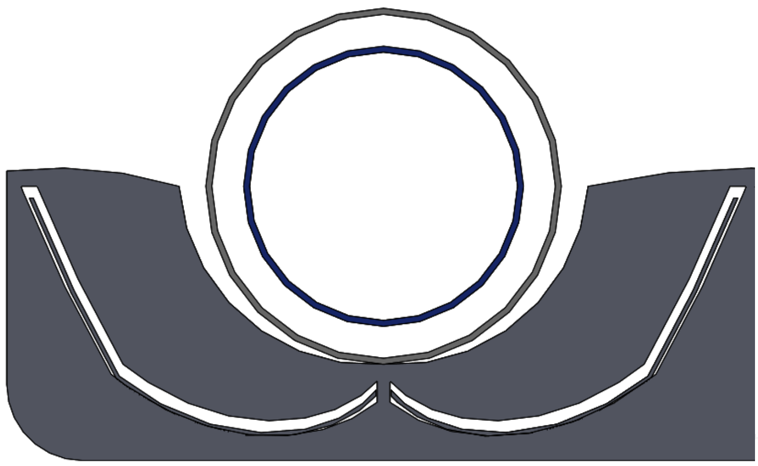

Figure 4.3 CPC rib which is used in the collector

A collector was made up by seven evacuated tube heat pipes and its manifold was designed at as small volume as possible which is 4 L. The collector has a width of of 650 mm and total aperture area of seven of CPC's is 1.166 m^2. The length of evacuated tube is of 1980 mm; however, 180 mm is inside the manifold. Then, the manifold was insulated with polyurethane foam and covered with aluminum sheet metal in a rectangular form. The non-insulated manifold is illustrated in Figure 4.4 and the final view of manifold can be seen in Figure 4.5 and Figure 4.6.

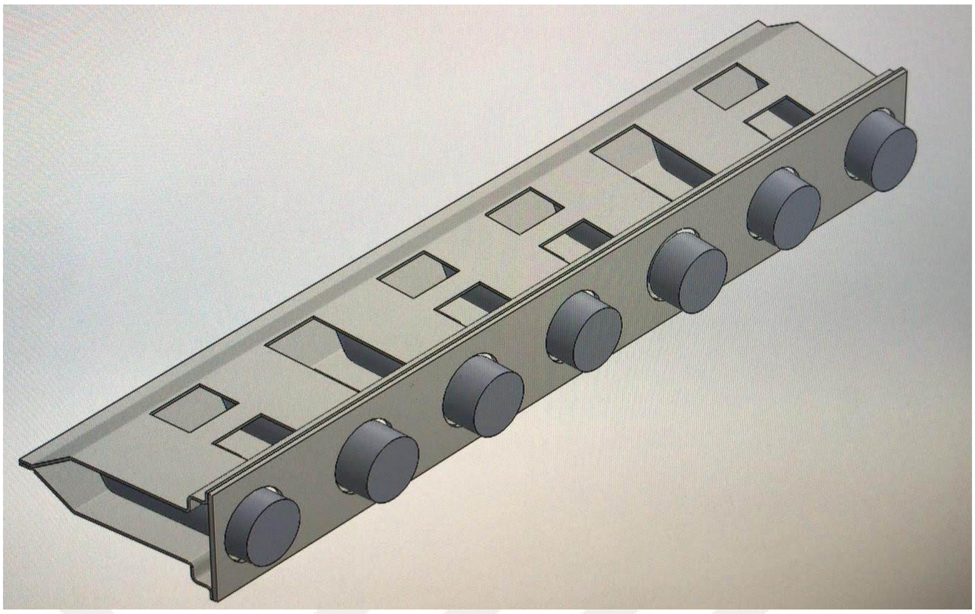

Figure 4.4 Skeleton structure of the collector's manifold

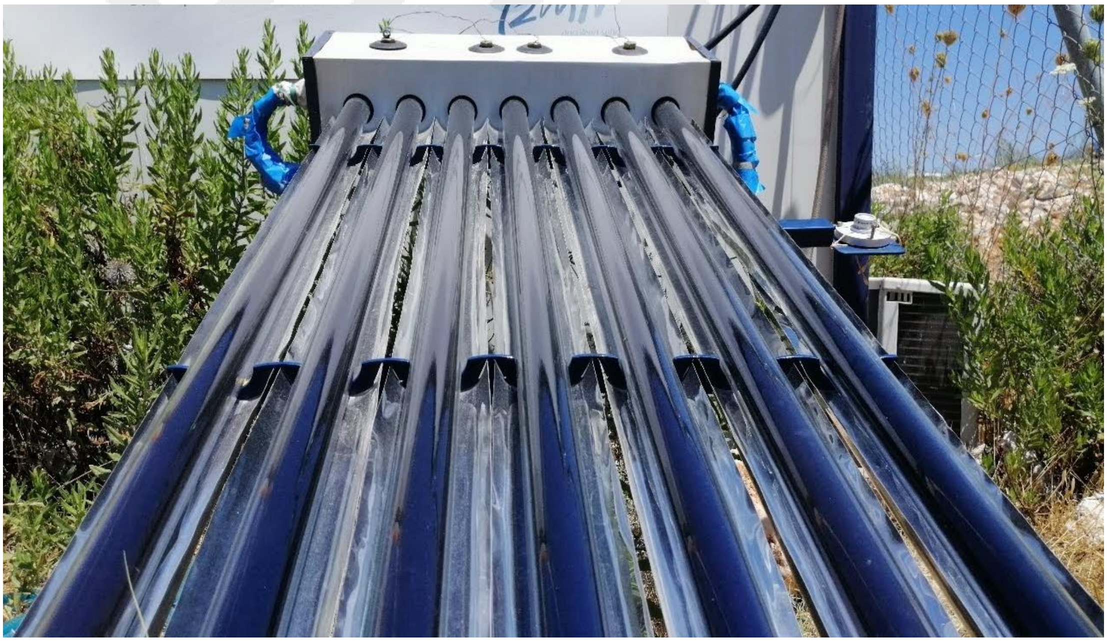

Figure 4.5 Front view of CPC (Personal archive, 2019)

Figure 4.6 Right-side view of CPC (Personal archive, 2019)

4.2 Experimental Setup

The slope angle of the collector is 23° and it was faced towards south. The CPC was placed in Buca, Izmir where the coordinates are 38°22’03.1’’N and 27°12’13.3’’E. The all system includes evacuated tube heat pipes, manifold, balance tank and a circulating water bath. Hot water circulator bath was used in order to feed water at constant temperature to the inlet of the collector’s manifold.

Global irradiation measurement was performed with LP Silicon PYRA-04 pyranometer which is placed at collector’s slope angle (23°) and it has an uncertainty of 3%. Temperature measurements were carried out with T type thermocouples which have an uncertainty of ±0.5°C. All the measurement instruments were connected to Agilent 34972A data logger. Flow rate measurement was accomplished with constant volume container of 0.5 L; uncertainty of volume measurement is 5 mL and uncertainty of filling time is 0.5 s.

Hose connections were made between the collector, water tank and pump. Connections were made leak-proof with PTFE tape (Polytetrafluoroethylene) which is supported with hose clamp. After the completion of collector's installation, a few tests were carried out due to leaking and circulation. Temperature measurements were carried out at seven different points which are inlet, outlet, outdoor and four points in the manifold. Four of the thermocouples were placed in thermowells. Thermowell is an element to protect the thermocouples inside of it from the working fluid. In utilization, it is filled with oil so that oil is heated by conduction in a steady way. Thermocouples read the temperatures correctly, without fluctuation. In the experiment, thermowells were place to manifold, at four different points.

The water tank which has a capacity of 4 L and it was hanged to higher height in comparison with the collector; in this way, water can flow naturally by the effect of gravity. The tank was cut 3 screw threads for inlet, outlet and pump feedback. Screw threads were mounted with 1/2-inch hose nipples. Collector feeding outlet was supported with throttle valve in order to regulate flow rate. General overview of experimental setup was shown in Figure 4.7.

Figure 4.7 Experimental setup (Personal archive, 2019)

4.3 Operation of the Experiment

As it is said, the experimental model was made of a pump, water tank and the CPC with evacuated tube heat pipes. The pump has reservoir with a heater so that temperature of feed water to collector can be arranged. The working fluid, water, is poured to the reservoir and it is pumped to water tank with 4 L/min (max flow rate of pump) and the throttle valve at the outlet of tank was nearly off so that the tank can be full of water and water can be fed back to the pump. After the circulation between the pump and the tank has not any problem, the throttle valve is made on and water can be fed to the collector's manifold.

The circulation between the pump, the tank and the collector has to work properly. The throttle valve can be adjusted in terms of required flow rate. Flow rate was measured with measuring cylinder by filling the cylinder with collector's outlet water whose hose was supported with a hose carrier so that water flows down to the circulation bath from higher location.

In Figure 4.8, the operation principle is schematically given. First of all, water is pumped to the balance tank, then water is regulated with a throttle valve and fed to collector. Excessive water in the tank is recirculated back to circulation bath. After that, water passing through the collector's manifold is heated with solar irradiance and leaves the manifold as hot water. In Figure 4.8; M is for collector manifold, D is for data logger, Pyr is for pyranometer, P is for pump, B is for balance tank, C is for circulation bath, V is for throttle valve and T is for thermocouple. In the experiment seven thermocouples were used and named as in the following; T7 as ambient temperature, T1 and T6 as outlet and inlet temperatures of manifold, T2, T3, T4 and T5 as temperatures in different points of manifold.

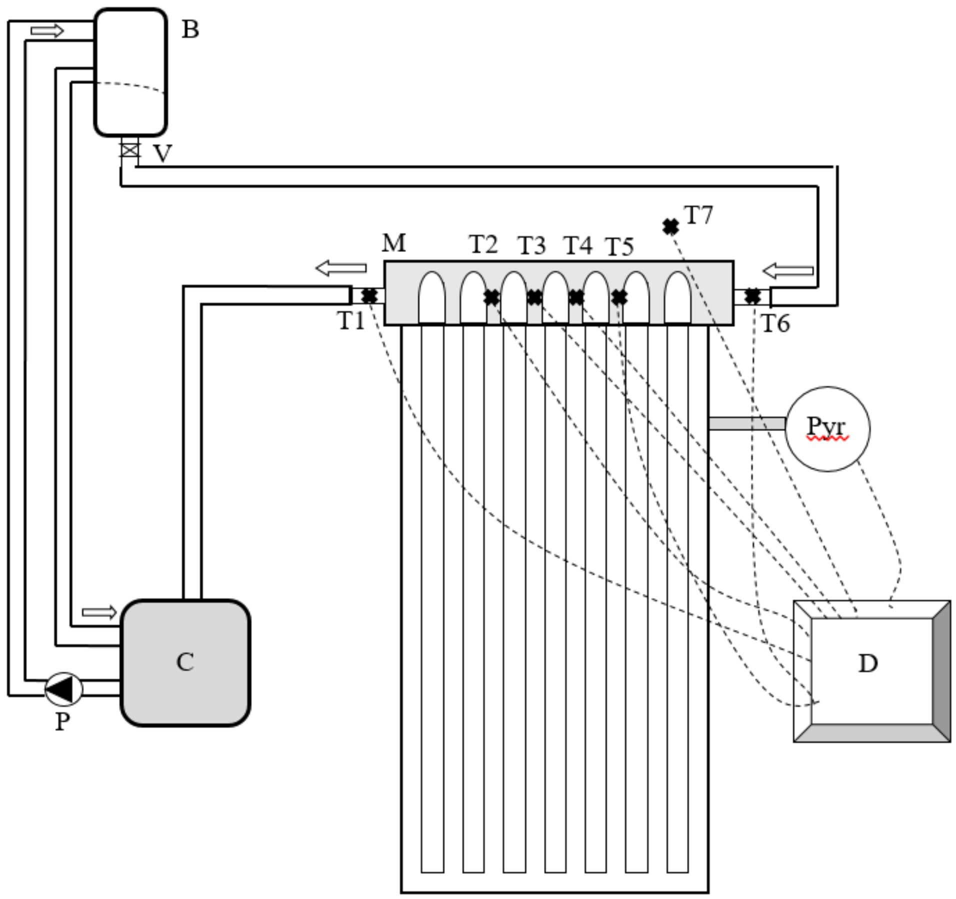

Figure 4.8 Schematic drawing of experimental setup

4.4 Experiments

Four experiments were carried out under similar solar intensities; inlet and outlet temperature of working fluid, ambient temperature and solar irradiation was measured. Measurements were taken per minute and recorded between 12:00 and 14:00 according to the standard time.

4.4.1 Experiment-1

Experiment-1 was conducted in July 22nd and it lasted for 120 minutes. Inlet and outlet temperature of water, ambient temperature and solar irradiation were demonstrated in Figure 4.9. The solar irradiation has an average value of 900.56 W/m^2. Volumetric flow rate was 1.2 L/min. Water inlet temperature was kept between 50°C to 58°C. Outlet temperature of water changed depending on the intensity of solar irradiation. As it is seen, the temperature difference of water between inlet and outlet is 6.70°C average.

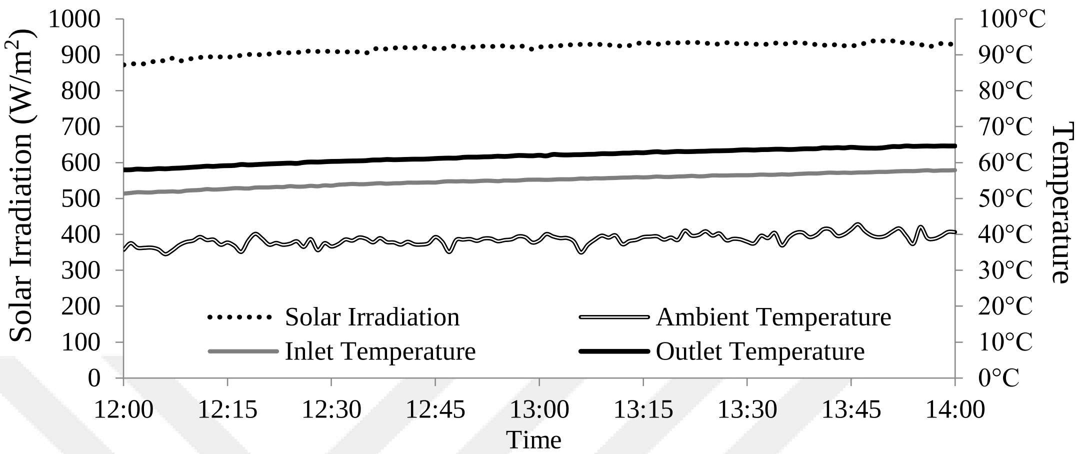

Figure 4.9 Solar irradiation and inlet, outlet, ambient temperature in Experiment-1

In Figure 4.10, the average rate of solar energy was measured as 1050.05 W and the average rate of energy transfer to water was measured as 560.08 W during the test.

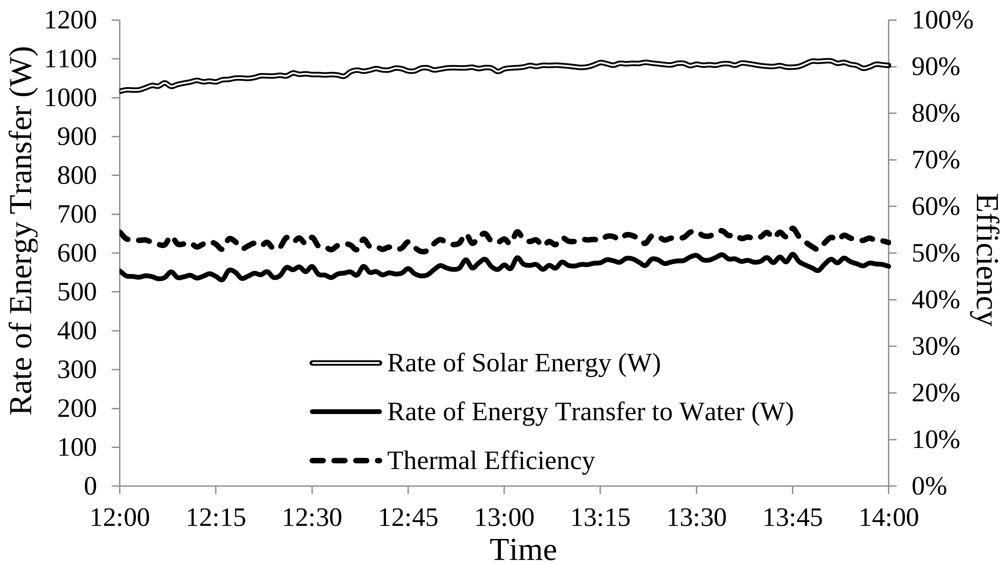

Figure 4.10 Optical and thermal efficiency, rate of energy transfer to water and rate of solar energy in Experiment-1

4.4.2 Experiment-2

Experiment-2 was conducted in July 23rd and it lasted for 120 minutes. Inlet and outlet temperature of water, ambient temperature and solar irradiation were demonstrated in Figure 4.11. The solar irradiation has an average value of 875.32 W/m^2. Volumetric flow rate was 1.08 L/min. Water inlet temperature was kept between 52°C to 56°C. Outlet temperature of water changed depending on the intensity of solar irradiation. As it is seen, the temperature difference of water between inlet and outlet is 6.25°C average.

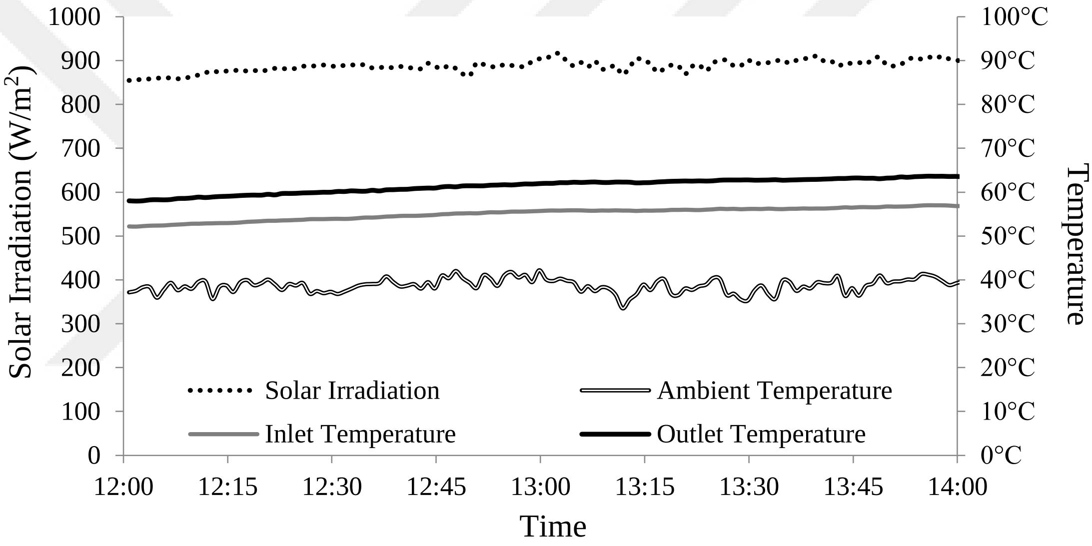

Figure 4.11 Solar irradiation and inlet, outlet, ambient temperature in Experiment-2

In Figure 4.12, the average rate of solar energy was measured as 1020.62 W and the average rate of energy transfer to water was measured as 470.48 W during the test.

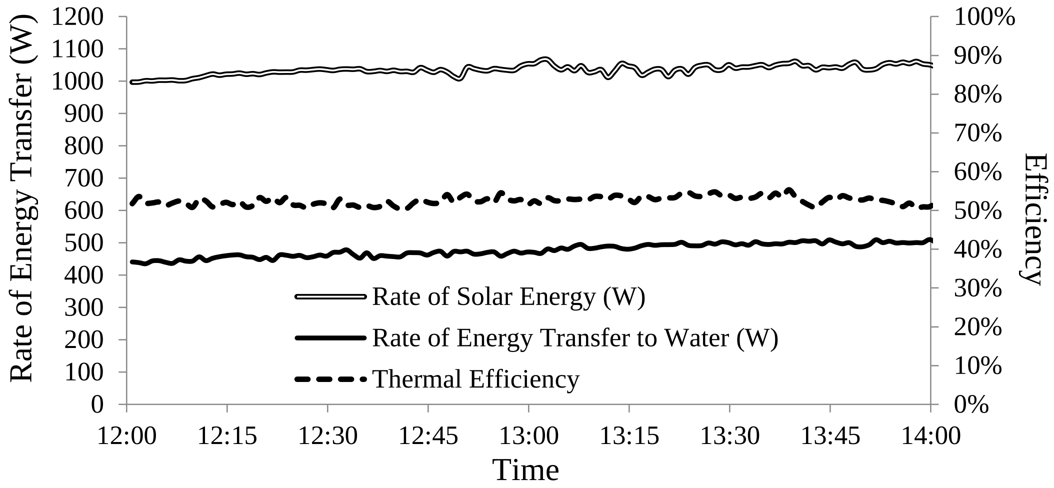

Figure 4.12 Optical and thermal efficiency, rate of energy transfer to water and rate of solar energy in Experiment-2

4.4.3 Experiment-3

Experiment-3 was conducted in July 25th and it lasted for 120 minutes. Inlet and outlet temperature of water, ambient temperature and solar irradiation were demonstrated in Figure 4.13. The solar irradiation has an average value of 900.96 W/m^2. Volumetric flow rate was 1.17 L/min. Water inlet temperature was kept between 69°C and 70°C. Outlet temperature of water changed depending on the intensity of solar irradiation. As it is seen, the temperature difference of water between inlet and outlet is 7.02°C average.

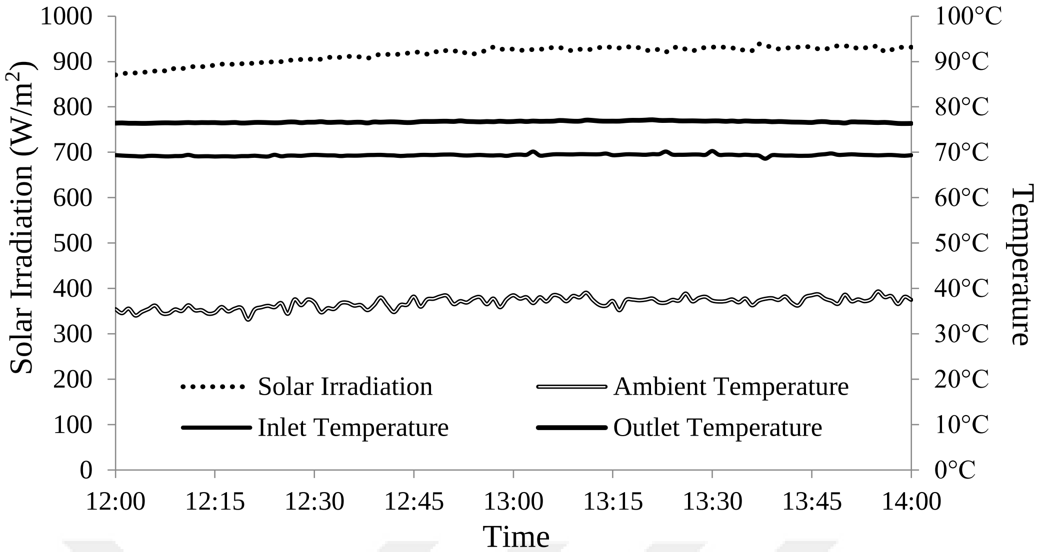

Figure 4.13 Solar irradiation and inlet, outlet, ambient temperature in Experiment-3

In Figure 4.14, the average rate of solar energy was measured as 1050.51 W and the average rate of energy transfer to water was measured as 572.36 W during the test.

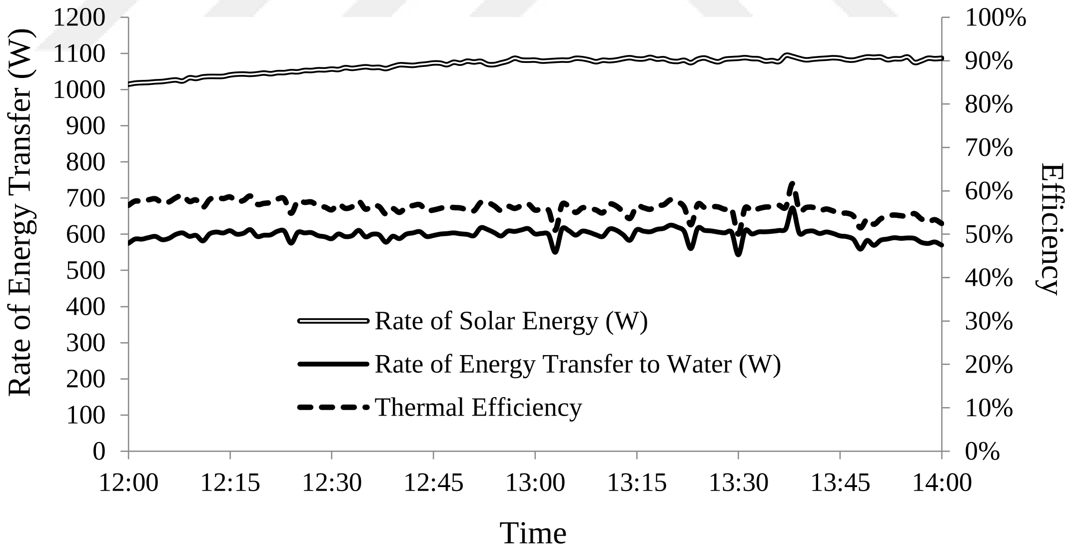

Figure 4.14 Optical and thermal efficiency, rate of energy transfer to water and rate of solar energy in Experiment-3

4.4.4 Experiment-4

Experiment-4 was conducted in July 26th and it lasted for 120 minutes. Inlet and outlet temperature of water, ambient temperature and solar irradiation were demonstrated in Figure 4.15. The solar irradiation has an average value of 882.75 W/m^2. Volumetric flow rate was 1.29 L/min. Water inlet temperature was kept at ~78°C. Outlet temperature of water changed depending on the intensity of solar irradiation. As it is seen, the temperature difference of water between inlet and outlet temperature is 6.43°C average.

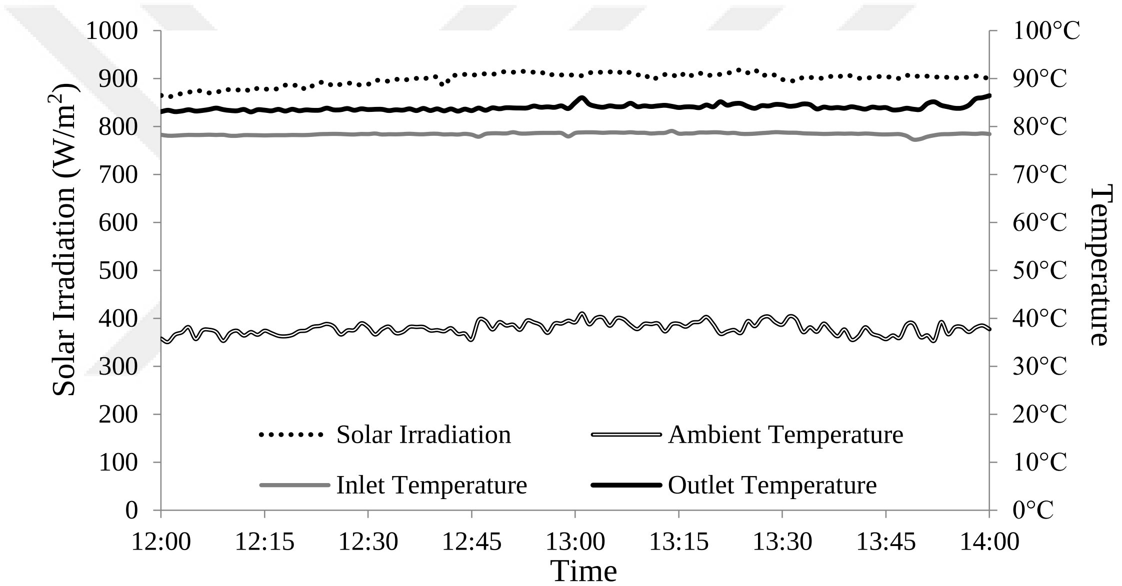

Figure 4.15 Solar irradiation and inlet, outlet, ambient temperature in Experiment-4

In Figure 4.16, the average rate of solar energy was measured as 1029.28 W and the average rate of energy transfer to water was measured as 577.64 W during the test.

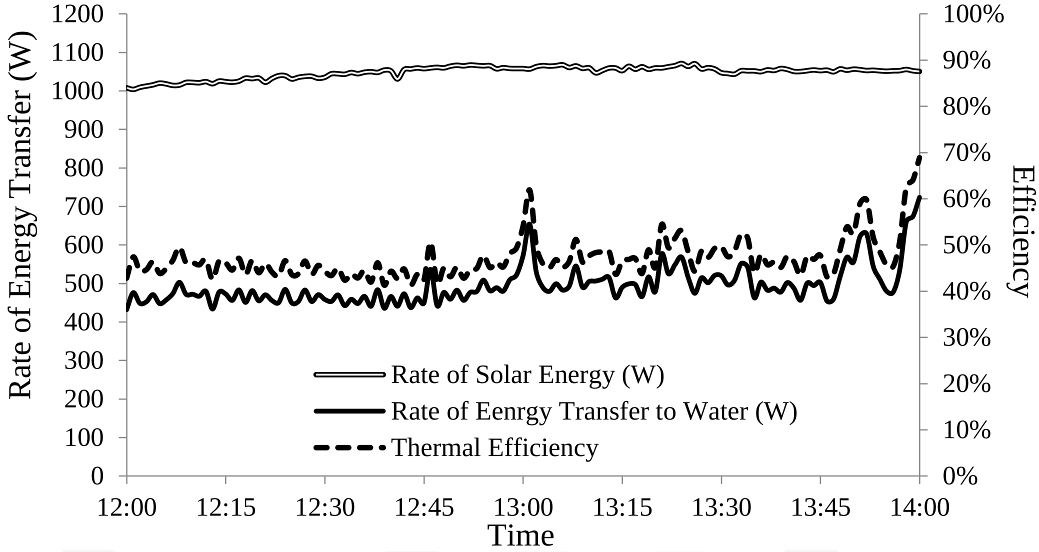

Figure 4.16 Optical and thermal efficiency, rate of energy transfer to water and rate of solar energy in Experiment-4

4.5 Evaluation of the Experimental Results

In Experiment-1, the total solar energy to the collector’s surface during the experiment is 2141.69 Wh and the total transferred energy to water is 1127.13 Wh. In this case, the thermal efficiency of experiment is 52.6%.

In Experiment-2, the total solar energy to collector’s surface during the experiment is 2069.48 Wh. The total transferred energy to water is 953.80 Wh. The thermal efficiency of the experiment is 46.1%.

In Experiment-3, the total solar energy to collector’s surface during the experiment is 2136.93 Wh. The total transferred energy to water is 1197.52 Wh. The thermal efficiency of the experiment is 56.0%.

In Experiment-4, the total solar energy to collector’s surface during the experiment is 2096.05 Wh. The total transferred energy to water is 988.83 Wh. The thermal efficiency of the experiment is 47.2%.

For all four experiments, the values of total solar energy to collector's surface and total transferred energy to water were illustrated in Figure 4.17.

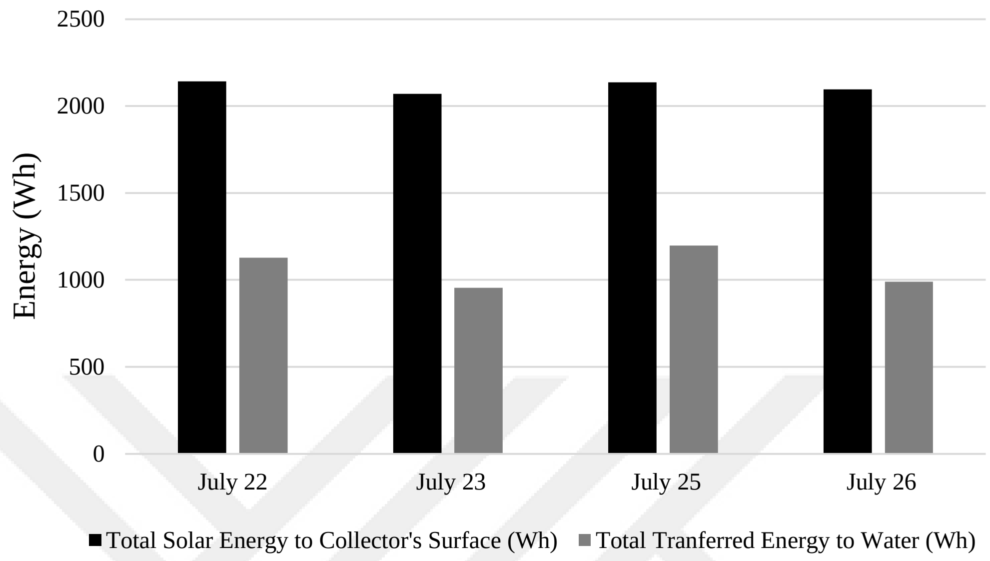

Figure 4.17 Comparison of energy transfer in the experiments

Thermal efficiencies of Experiment-1, Experiment-2, Experiment-3 and Experiment-4 were given in Figure 4.18. Thermal efficiencies in the experiments were changed between 46.1% and 56%. In addition, optical efficiency is 67% for all experiments.

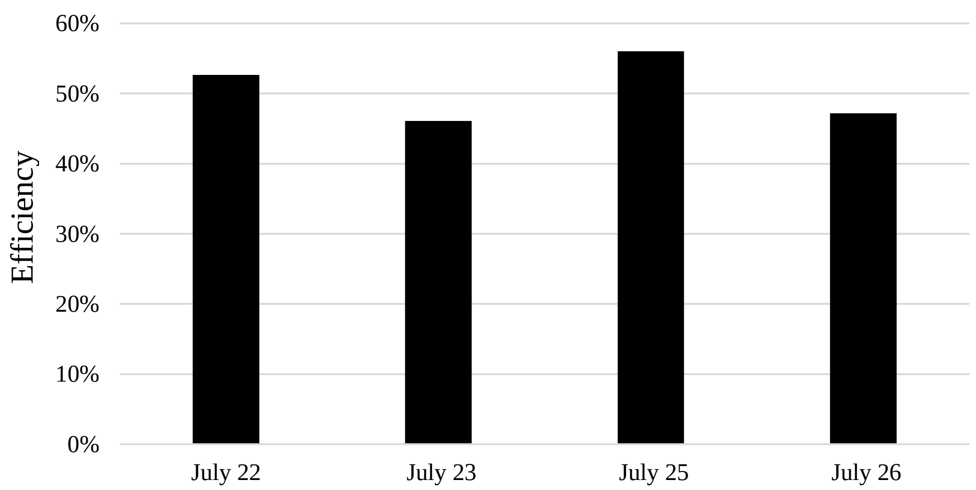

Figure 4.18 Comparison of thermal efficiencies in the experiments

4.6 Uncertainty Analysis

Uncertainty analysis allows researchers to identify the percentage of certainty of an experimental study. Measurement methods include different errors which are measurement technique, measurement tool and timing can make a vital effect to the result. (Gao, Fan, Zhang, An, Wang, Gao & Yu, 2014) gave an expression in order to calculate the overall uncertainty in Eq. (4.1).

$$W_R = \left[\left(\frac{\partial R}{\partial x_1} w_1 \right)^2 + \left(\frac{\partial R}{\partial x_2} w_2 \right)^2 + \left(\frac{\partial R}{\partial x_3} w_3 \right)^2 \right]^{\frac{1}{2}} \quad (4.1)$$

In Eq. (4.1), R is the dimension of measurement, W_R is the total error rate, w_n is the error rate of independent variable, x_n is the deviation affecting the measurement.

In the experiments, irradiation was measured with a silicon type pyranometer with an uncertainty of 3% at displayed value and solar energy gain in the aperture area (E_{solar}) has an uncertainty of 3%.

The energy transferred to water was calculated as in Eq. (4.2). In Eq. (4.2), $\dot{m}_{water}$ is mass flow rate of water (kg/s), $C_{p_{water}}$ is the specific heat of water (J/kg.K), $T_{water,out}$ is the temperature of outlet water (K) and $T_{water,in}$ is the temperature of outlet water (K).

$$\dot{Q}_{flow} = \dot{m}_{water} \cdot C_{p_{water}} \cdot \left(T_{water,out} - T_{water,in}\right) \quad (4.2)$$

C_p is specific heat and has a constant value. Type T thermocouples were connected to an Agilent 34972A model data logger which has a measurement uncertainty of ±0.5°C. The temperature uncertainty of water between manifold's inlet and outlet is calculated as ±0.71°C. On calculation of the volumetric flow rate, the uncertainty of the volume is 5 mL of a 500 ml scale cap and time measurement has an uncertainty of 0.5 s.

In Experiment-1, temperature difference was measured as 6.7°C and uncertainty of temperature difference is 10.6%. The amount of water filled in the scale cap is 200 mL and filling duration is 10 s. The uncertainty of volumetric flow rate is calculated 5.6%.

In Experiment-2, temperature difference was measured as 6.25°C and uncertainty of temperature difference is 11.4%. The amount of water filled in the scale cap is 180 ml and filling duration is 10 s. The uncertainty of volumetric flow rate is calculated 5.7%.

In Experiment-3, temperature difference was measured as 7.02°C and uncertainty of temperature difference is 10.1%. The amount of water filled in the scale cap is 195 ml and filling duration is 10 s. The uncertainty of volumetric flow rate is calculated 5.6%.

In Experiment-4, temperature difference was measured as 6.43°C and uncertainty of temperature difference is 11.0%. The amount of water filled in the scale cap is 215 ml and filling duration is 10 s. The uncertainty of volumetric flow rate is calculated 5.5%.

The uncertainty of transferred energy to water for the Experiment-1, Experiment-2, Experiment-3 and Experiment-4 is calculated as 11.99%, 12.75%, 11.55% and 12.30%, respectively.

CHAPTER FIVE

ANNUAL PERFORMANCE COMPARISON OF EVACUATED TUBE WITH AND WITHOUT REFLECTOR

In this chapter, a comparison was made between evacuated tube with and without reflector. Reflector's is made of compound parabolic. This comparison includes annual optical analysis of evacuated tube with and without compound parabolic reflector. Annual optical analysis gives a projection of harvestable solar energy.

5.1 Analysis of the CPC and Evacuated Tube

The CPC which will be analyzed is as it was shown in Figure 3.11. According to this, evacuated tube is made of concentric and co-axial two glass tubes. The outside surface of inner tube is coated with Al-N/Al as selective surface. It has an inner diameter of 37 mm and outer diameter of 47 mm. The wall thickness of the glasses is 1.3 mm and the length of the tubes is 1800 mm. Outer tube has a transmission coefficient of 0.90 and inner tube has an absorptivity of 0.925.

For the specified evacuated tube, a compound parabolic reflector was designed which has 30° acceptance half angle. The reflector's height was truncated down to 87% as shown in Figure 3.11. The coefficient of reflection is 0.80. The optical efficiency of CPC was made for the incidence angle of 0° to 90° with 5° intervals and it was illustrated in Figure 3.18. The proposed design has an average optical efficiency of 70.32%. On the other hand, the evacuated tube without reflector has constant optical efficiency of 83.25% during the day, in terms of coefficient of reflection and absorption.

5.2 Calculation of Absorbed Energy

It has to be taken into account that the time dependent alteration of incidence angle of sun rays and intensity of solar irradiation in order to calculate absorbed solar energy on evacuated tube with and without reflector. Figure 5.1 illustrates the values of intensity of solar irradiation for an average day in September which was taken from PVGIS. The location was input same as with the experiment location in Tınaztepe Campus of Dokuz Eylül University, Izmir. The slope angle and surface azimuth angle of the evacuated tube was accepted 35° and 0°, respectively.

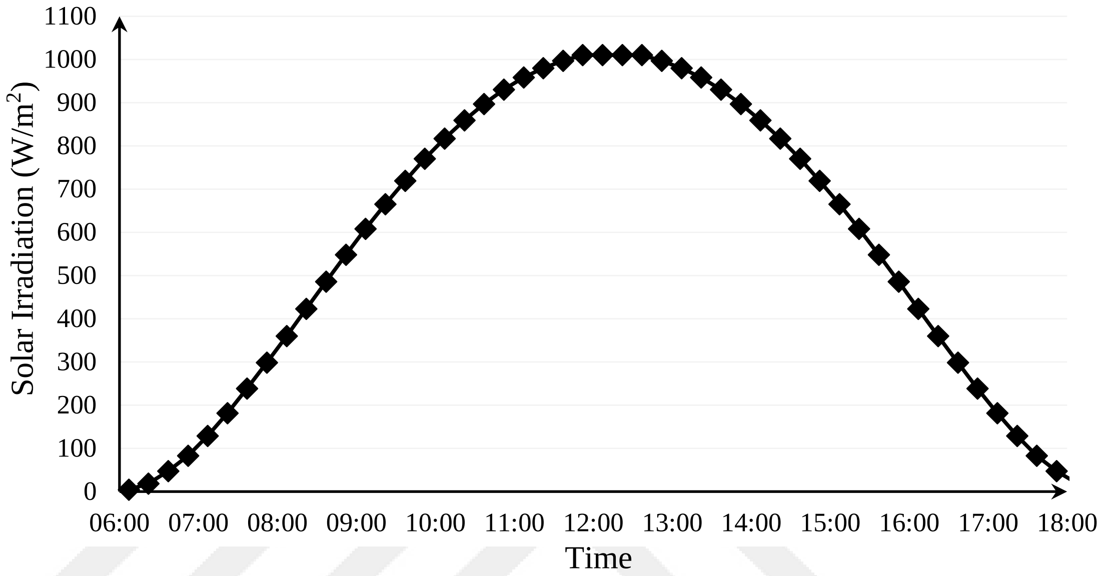

Figure 5.1 The alteration of intensity of solar irradiation during the day (September)

The total amount of absorbed solar energy was calculated separately for evacuated tube with and without reflector. In Eq. (5.1), P, I_{solar}, $A_{aperture}$ and $\eta_{optical}$ represent the instant power of evacuated tube with and without reflector, the intensity of solar irradiation, aperture area of the collector and the optical efficiency, respectively. In Eq. (5.2), E_{day} and Δt represent total absorbed energy during the day and time interval, respectively.

$$P = I_{solar} \cdot A_{aperture} \cdot \eta_{optical} \quad (5.1)$$

$$E_{day} = \sum P \cdot \Delta t \quad (5.2)$$

Applying the Eq. (5.2), the comparison was made for evacuated tube with and without reflector with given dimensions. Calculations show that a single evacuated tube with reflector which has 1800 mm length has an aperture area of 0.166 m^2 and the same single evacuated tube without reflector has a collecting area of 0.0666 m^2. In the evaluation of instant power of evacuated tube with reflector, the incidence angle of sun ray and instant the optical efficiency for the given incidence angle was taken into account. The alteration of instant power of evacuated tube with and without reflector was illustrated in Figure 5.2.

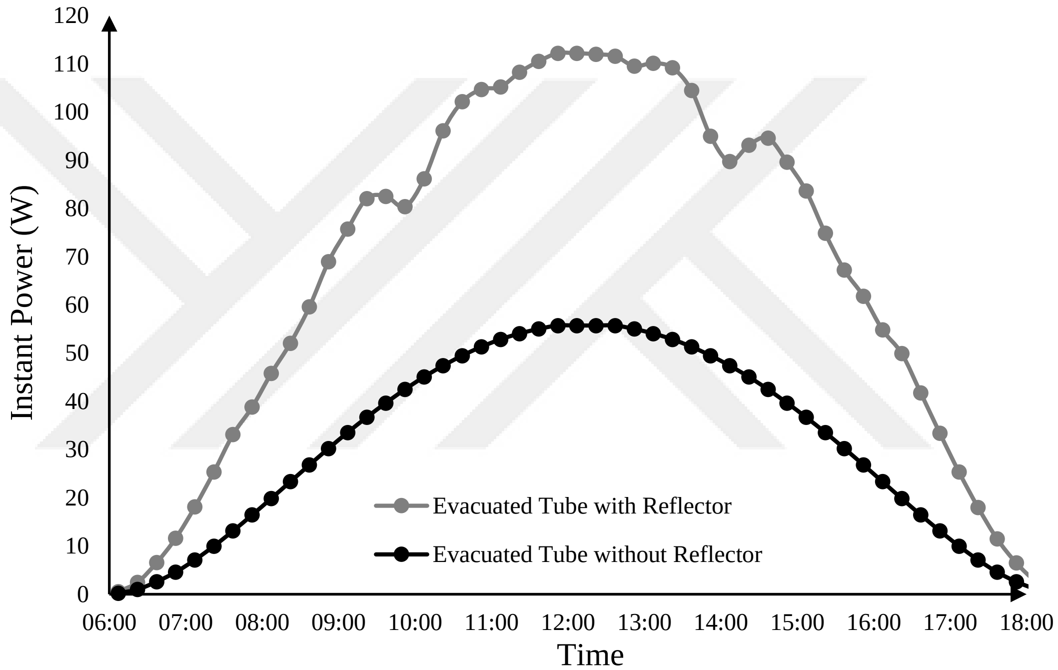

Figure 5.2 The alteration of instant power for evacuated tube with and without reflector in an average day in September

Daily amount of absorbed-solar energy can be calculated using Eq. (5.2). As a result of the study, comparing the potential of absorbed energy of evacuated tube with and without reflector, the effect of attached reflector can be seen in Figure 5.3. On an average day in September, the results revealed that the absorbed energy values are 0.818 kWh/day for evacuated tube with reflector, 0.387 kWh/day for evacuated tube without reflector. It is seen that attaching a compound parabolic reflector can increase the total absorbed energy up to 2.11 times.

Energy analysis was made in average days of all months. Figure 5.3 shows that the highest potential of absorbed energy is in June, July and August. In the average day of months, the ratio of daily energy for the tubes of a CPC is not below 2.08 times on the tube without reflector.

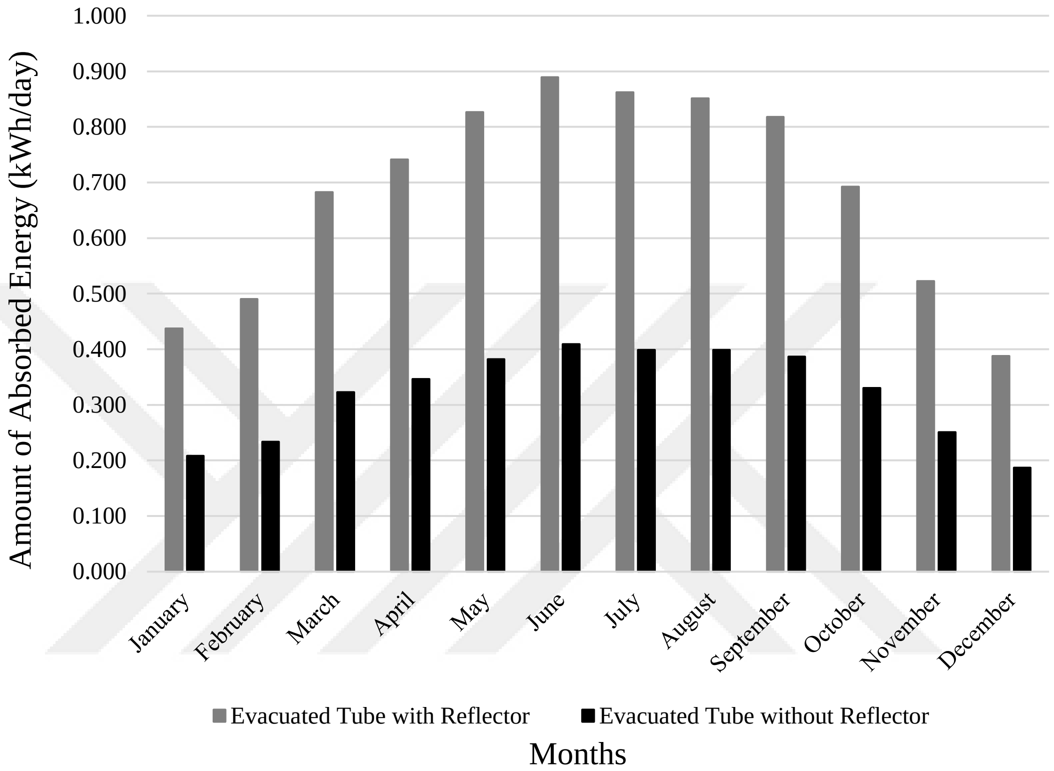

Figure 5.3 Monthly variation in potential of absorbed energy for an average day of all months

Figure 5.4 illustrates annual potential of the absorbed energy for an evacuated tube with and without reflector. It is seen that potential of absorbed energy is revealed for evacuated tube with and without reflector as 249.85 kWh and 117.43 kWh, respectively. By attaching a compound parabolic reflector increases the performance of traditional evacuated tube by 2.13 times.

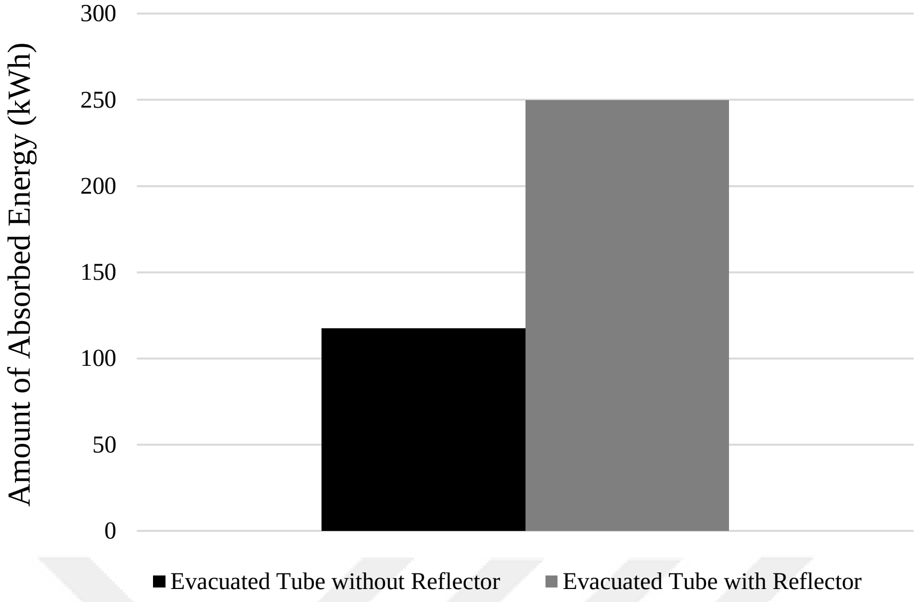

Figure 5.4 Annual potential of absorbed solar energy for evacuated tube with and without reflector

CHAPTER SIX
CONCLUSION

In this thesis, a CPC, which was made of an evacuated tube heat pipe as absorber, was designed and tested. The evacuated tube heat pipe gives the opportunity of decreasing the water volume in the CPC collector which allows the system to step in shorter time due to the mixture of ethanol inside the heat pipe. The tubular absorber's dimensions are 37 mm as inner diameter and 47 mm as outer diameter. The designed CPC has an aperture width of 92.55 mm and reflector height is 38.8 mm. By applying the ray analysis for rays which have different incidence angles, the optical efficiency was calculated. The optical efficiency yielded as 70.32%.

A prototype solar collector was made of 7 CPC's with evacuated tube heat pipes. It has a length of 1800 mm and width of 650 mm. In total, the CPC collector has an aperture area of 1.17 m^2. The collector was located with a slope angle of 23° and azimuth of 0° in Tınaztepe Campus of Dokuz Eylül University and tested in different weather conditions. During the tests, solar intensity and inlet and outlet temperatures were measured and transferred energy to water was calculated.

The Experiment-1 was accomplished in July 22nd. The average solar irradiation during the test was 900.56 W/m^2. The average temperature difference between inlet and outlet of manifold was 6.7°C for 1.2 L/min. The thermal efficiency of the Experiment-1 is 52.6%.

The average solar irradiation was 875.32 W/m^2 in Experiment-2. The experiment was accomplished in July 23rd. The average temperature difference between inlet and outlet of manifold was 6.25 for 1.08 L/min. The thermal efficiency of Experiment-2 was determined as 46.1%.

The Experiment-3 was carried out in July 25th. The solar irradiation was 900.96 W/m^2. The inlet temperature at the collector's manifold was 68°C. An average of

7.02°C temperature difference between inlet and outlet of the collector's manifold was reached for 1.17 L/min. The thermal efficiency of Experiment-3 is 56.0%.

The Experiment-4 was carried out in July 26th. The solar irradiation was 882.75 W/m^2. The inlet temperature at the collector's manifold was 78°C. 6.43°C temperature difference between inlet and outlet of the collector's manifold was reached for 1.29 L/min. The thermal efficiency of Experiment-4 is 47.2%.

In the experiments, thermal efficiency was changed between 46.1% and 56%, however, optical efficiency is 67%. As it is seen, heat loss was between 10% and 20% at working temperatures.

After that, the proposed CPC was examined in terms of optical efficiency for annual performance in comparison with evacuated tube without reflector. In results, the CPC and evacuated tube without reflector revealed an overall optical efficiency of 70.32% and 83.25%, respectively. Solar heat absorption capacity of the CPC is 249.85 kWh/year per one tube, and this is 213% of heat absorption capacity of evacuated tube without reflector. It is clear that adding a simple compound parabolic reflector increased the capacity of collecting solar energy as more than twice.

In conclusion, the experiments and optical analyzes show us that CPC's have a high efficiency in solar thermal energy production. The CPC is a promising area for hot water generation in the way of domestic and industrial use. Increasing of its share among traditional solar collectors is expected. Its low cost and easy-to-produce structure gives the opportunity of being popular in the solar collector market.

REFERENCES

Aguilar-Jiménez, J. A., Velázquez, N., Acuña, A., López-Zavala, R., & González-Uribe, L. A. (2018). Effect of orientation of a CPC with concentric tube on efficiency. *Applied Thermal Engineering*, *130*, 221–229.

Artic Solar. (n.d.). Retrieved December 12, 2019, from http://articsolar.com/applications/process-heat-hot-water-steam/

Baranov, V. K., & Melnikov, G. K. (1966). Study of the illumination characteristics of hollow focons. *Soviet Journal of Optical Technology*, (33), 408–411.

Bellos, E., Korres, D., Tzivanidis, C., & Antonopoulos, K. A. (2016). Design, simulation and optimization of a compound parabolic collector. *Sustainable Energy Technologies and Assessments*, *16*, 53–63.

Bellos, Evangelos, Tzivanidis, C., & Papadopoulos, A. (2018). Daily, monthly and yearly performance of a linear fresnel reflector. *Solar Energy*, *173* (August), 517–529.

Brogren, M. (2004). *Optical efficiency of low-concentrating solar energy systems with parabolic reflectors*. PhD Thesis, Uppsala University, Uppsala.

Buttinger, F., Beikircher, T., Pröll, M., & Schölkopf, W. (2010). Development of a new flat stationary evacuated CPC-collector for process heat applications. *Solar Energy*, *84* (7), 1166–1174.

Carvalho, M. J., Collares-Pereira, M., Gordon, J. M., & Rabl, A. (1985). Truncation of CPC solar collectors and its effect on energy collection. *Solar Energy*, *35* (5), 393–399.

Cooper, P. I. (1969). The absorption of radiation in solar stills. *Solar Energy*, *12* (3), 333–346.

Duffie, J. A., & Beckman, W. A. (2013). *Solar engineering of thermal processes* (4th ed.). New Jersey: John Wiley & Sons, Inc.

Essearth (2019). *Pyranometer*. Retrieved December 12, 2019, from http://www.essearth.com/product/pyranometers-from-kipp-zonen/

Gao, Y., Fan, R., Zhang, X. Y., An, Y. J., Wang, M. X., Gao, Y. K., & Yu, Y. (2014). Thermal performance and parameter analysis of a U-pipe evacuated solar tube collector. *Solar Energy*, *107*, 714–727.

Greenway CSP Solar Tower. (n.d.). Retrieved October 8, 2018, from http://www.yilsanholding.com/en-US/greenway/627285

Gudekar, A. S., Jadhav, A. S., Panse, S. V., Joshi, J. B., & Pandit, A. B. (2013). Cost effective design of compound parabolic collector for steam generation. *Solar Energy*, *90*, 43–50.

Günther, M., & Shahbazfar, R. (2011). *Advanced CSP teaching materials: solar dish technology* (1st ed.). Berlin: DLR Publications

Hinterberger, H., & Winston, R. (1966). Efficient light coupler for threshold Cerenkov counters. *Review of Scientific Instruments*, *37* (8), 1094–1095.

Huksefluxusa (2019). *Pyrheliometer*. Retrieved December 12, 2019, from htttp://www.huksefluxusa.com/shop/applications/pv-monitoring-solar-resource-assessment/dr01-pyrheliometer/

Jadhav, A. S., Gudekar, A. S., Patil, R. G., Kale, D. M., Panse, S. V., & Joshi, J. B. (2013). Performance analysis of a novel and cost effective CPC system. *Energy Conversion and Management*, *66*, 56–65.

Jiang, L., Widyolar, B., & Winston, R. (2015). Characterization of novel mid-temperature CPC solar thermal collectors. *Energy Procedia*, *70*, 65–70.

Kalogirou, S. (2009). *Solar energy engineering - processes and systems* (1st ed.). Amsterdam: Elsevier.

Kim, Y., Han, G. Y., & Seo, T. (2008). An evaluation on thermal performance of CPC solar collector. *International Communications in Heat and Mass Transfer*, *35* (4), 446–457.

Kipp & Zonen Brochure. (n.d.). Retrieved December 12, 2019, from https://www.kippzonen.com/Download/358/Brochure-Pyranometers-SP-Lite2-English?ShowInfo=true

Klein, S. A. (1977). Calculation of monthly average insolation on tilted surfaces. *Solar Energy*, *19* (4), 325–329.

Liu, Z., Tao, G., Lu, L., & Wang, Q. (2014). A novel all-glass evacuated tubular solar steam generator with simplified CPC. *Energy Conversion and Management*, *86*, 175–185.

Lucida Solar. (n.d.). Retrieved October 4, 2018, from https://lucidasolar.com/

McIntire, W. R. (1979). Truncation of nonimaging cusp concentrators. *European Journal of Applied Microbiology and Biotechnology*, *23*, 351–355.

Rabl, A., O'Gallagher, J., & Winston, R. (1980). Design and test of non-evacuated solar collectors with compound parabolic concentrators. *Solar Energy, 25* (4), 335-351.

Rabl, Ari. (1976). Comparison of solar concentrators. *Solar Energy*, *18* (2), 93–111.

Santos-González, I., Sandoval-Reyes, M., García-Valladares, O., Ortega, N., & Gómez, V. H. (2014). Design and evaluation of a compound parabolic concentrator for heat generation of thermal processes. *Energy Procedia*, *57*, 2956–2965.

Shah, P. K., Srinivasan, K., & Murthy, S. S. (1990). Geometry of ideal CPC collectors with gap between absorber and reflector. *International Journal of Solar Energy*, *9* (1), 13–21.

Singh, H., Redpath, D. A. G., Aboutorabi, A., Kattakayam, T. A., & Griffiths, P. W. (2010). Optimum configuration of compound parabolic concentrator (CPC) solar water heater types for dwellings situated in the northern maritime climate. *International Journal of Ambient Energy*, *31* (1), 47–52.

Sistem Tubular Online Catalogue. (n.d.). Retrieved December 23, 2018, from http://sistemtubular.com.tr/wp-content/uploads/2018/e-katalog-tr.pdf

Solar Spectrum. (n.d.). Retrieved May 16, 2019, from https://www.agga.org.au/technical/technical-fact-sheets/

Solar System. (n.d.). Retrieved July 18, 2019, from https://solarsystem.nasa.gov/solar-system/sun/in-depth/

Sonawane, P. D., & Bupesh Raja, V. K. (2017). An overview of concentrated solar energy and its applications. *International Journal of Ambient Energy*, *39* (8), 898–903.

Spencer, J. V. (1971). Fourier series representation of the position of the sun. *Search*, *2* (5), 172–174.

Taylor, P., Manikumar, R., & Arasu, A. V. (2014). An analytical and experimental study of the linear fresnel reflector solar concentrator system. *Distributed Generation & Alternative Energy Journal*, 29 (2), 52-80.

Tiwari, A., & Shyam. (2016). *Handbook of solar energy* (1st ed.). Berlin: Springer.

Ustaoglu, A., Okajima, J., Zhang, X. R., & Maruyama, S. (2016). Evaluation of the efficiency of dual compound parabolic and involute concentrator. *Energy for Sustainable Development*, *32*, 1–13.

Wang, J., Yu, L., Jiang, C., Yang, S., & Liu, T. (2016). Optical analysis of solar collector with new V-shaped CPC. *Solar Energy*, *135*, 780–785.

Wang, P. Y., Li, S. F., & Liu, Z. H. (2015). Collecting performance of an evacuated tubular solar high-temperature air heater with concentric tube heat exchanger. *Energy Conversion and Management*, *106*, 1166–1173.

Widyolar, B., Jiang, L., Ferry, J., & Winston, R. (2018). Non-tracking east-west XCPC solar thermal collector for 200 celsius applications. *Applied Energy*, *216*, 521–533.

Winston, R. (1974). Principles of solar concentrators of a novel design. *Solar Energy*, *16* (2), 89–95.